Durham E-Theses

Some properties of rare earth doped soda glass.

Curry, J. R.

How to cite:

Curry, J. R. (1971) *Some properties of rare earth doped soda glass.*, Durham theses, Durham University. Available at Durham E-Theses Online: http://etheses.dur.ac.uk/10030/

Use policy

SOME PROPERTIES OF RARE EARTH

DOPED SODA GLASS.

by

J. R. CURRY.

Presented in candidature for the degree

of Master of Science.

August 1971.
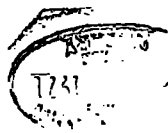
ACKNOWLEDGMENTS.

The author wishes to express his thanks to

Professor G.D. Rochester, who made the facilities

of his department available for this research.

He also gratefully appreciates the help of

Dr. K.N.R. Taylor who has offered valuable

assistance in the interpretation of the results.

ABSTRACT.

To ascertain which properties are sensitive to a crystalline

environment about the constituent ions of a normal glass, or included

impurity ions, prepared specimens were subjected to a variety of

experimental techniques. Measurements were made on soda glasses doped with

the elements of the rare earth series using the following techniques:

(i)   X-Ray Diffraction Spectra;

(ii)   Conductivity (ionic) Measurements;

(iii)   Magnetic Susceptibility Measurements;

(iv)   Optical Absorption Spectra;

(v)   Electron Spin Resonance.

As a result of these measurements it is clear that, for a study of glass

systems using rare earth probes, experiments involving either optical

or E.S.R. measurements will provide most information about the glass matrix.

The electrical conductivity is less likely to provide direct

structural information since its value depends upon so many parameters.

However, the observed dependence of the resistivity on the ionic moment

of the dissolved ions is extremely interesting and requires further

investigation.

CONTENTS.

CONTENTS. (contd.)

CONTENTS.(contd.)

CHAPTER ONE.

INTRODUCTION.

1.1 The Structure of Glasses.

Our present understanding of the structure of glass

rests largely on the concepts introduced by W.H.Zachariasen

in 1932 (1)*.

Contemporary research into the structure of crystalline

silicates by W.L.Bragg (2) had revealed that, in every case,

the silicon atom is tetrahedrally bonded to four oxygens at

a distance of 1.62A. Zachariasen reasoned that, since the

intrinsic strength of glass is of the same order as that of

crystals, the inter-atomic bonding forces in a glass must

be of the same nature as those in the crystal form. In the

case of silicate glasses he proposed that each silicon would

be surrounded by an oxygen polyhedron as expected but these

polyhedra would share only corners (not edges or planes) with

each other. In a three dimensional network the polyhedra

would share at least three corners with other polyhedra. The

result, shown diagrammatically in Figure 1.1a, is an irregular

network having an energy content comparable with the

corresponding crystal.

* Numbers in brackets indicate references on page 64.
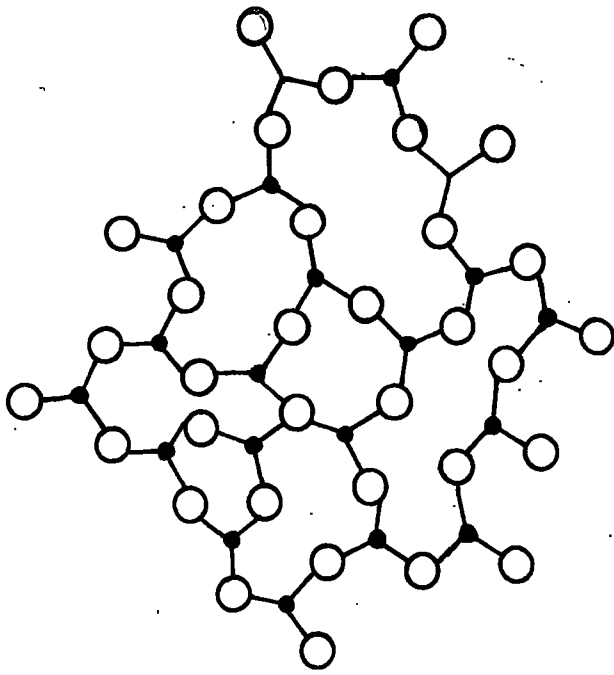
A GLASS.

FIG. 1.1a
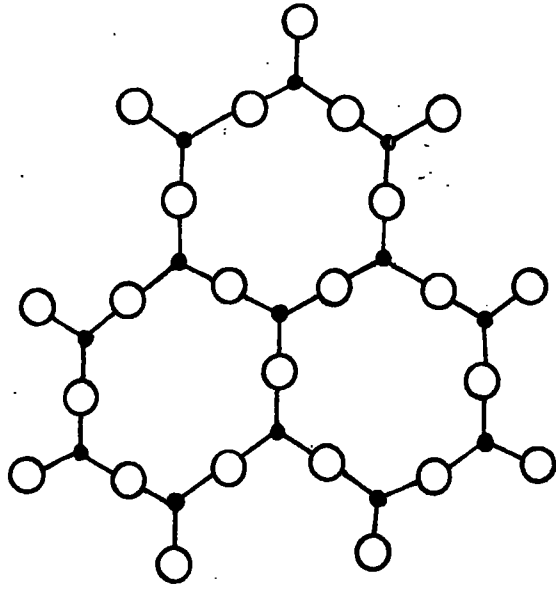
A CRYSTAL.

FIG. 1.1b

SCHEMATIC REPRESENTATION IN TWO DIMENSIONS OF THE
DIFFERENCE BETWEEN A GLASS AND A CRYSTAL.
(ZACHARIASEN.)

The lack of symmetry and periodicity is in strong contrast with the regular arrangement in the crystalline state (Figure 1.1b), and immediately leads to several consequences, which are characteristic of glasses. In the first place, the solid glass is isotropic, which immediately follows from the lack of symmetry. In the second place, if a glass consists of several different constituents (as is the case in inorganic oxide-glasses) it is, generally speaking, not possible to express the chemical composition by a simple formula. This is due to the lack of periodicity of the network in glasses, in contrast with that of crystals, in which the composition of one unit cell defines the chemical composition. In the third place, the atoms or molecules of the same kind, composing the vitreous network, are not all equivalent, as is the case in a crystal lattice.

The energy required to break one of the chemical bonds which hold the network together will be different for each individual link, though, of course, for the majority of bonds of the same type these energy values will not differ greatly from a certain average value. Therefore, the breakdown of the network with increasing temperature will be a gradual one, corresponding to gradual liquifaction.

The random network theory of Zachariasen was in conflict with a suggestion, put forward by Randall (3) in

1930, that glasses are formed from aggregates of microscopic crystals. This crystallite theory, as it became known, was based upon X-ray studies of vitreous silica and the equivalent crystalline form, cristobalite. Comparing the X-ray diffraction patterns of the two (Figure 1.2a and Figure 1.2b), the first broad peak of the vitreous silica corresponds to the strongest ring of the cristobalite. Since the line breadth is known to increase as the size of the crystalline particle decreases, a pattern similar to that obtained for vitreous silica is to be expected for a microcrystalline structure. In order to explain the observed peak width, the crystallite size would have to be in the order of $7.7\overset{o}{A}$ which is scarcely larger than one unit cell of cristobalite.

Fundamental to the concept of crystallinity is long range atomic order repetition, and in a particle containing only one unit cell repetition cannot exist. There was then a very real objection to the cristobalite crystallite description of silica glass. In order to conform to the experimental facts, it required the extension of the term "crystal" to blocks of matter so small that the term no longer had any meaning.

A modification of the crystallite theory proposed by Valenkov et al (4) in 1936 proved more realistic. They

(a) CRISTOBALITE.
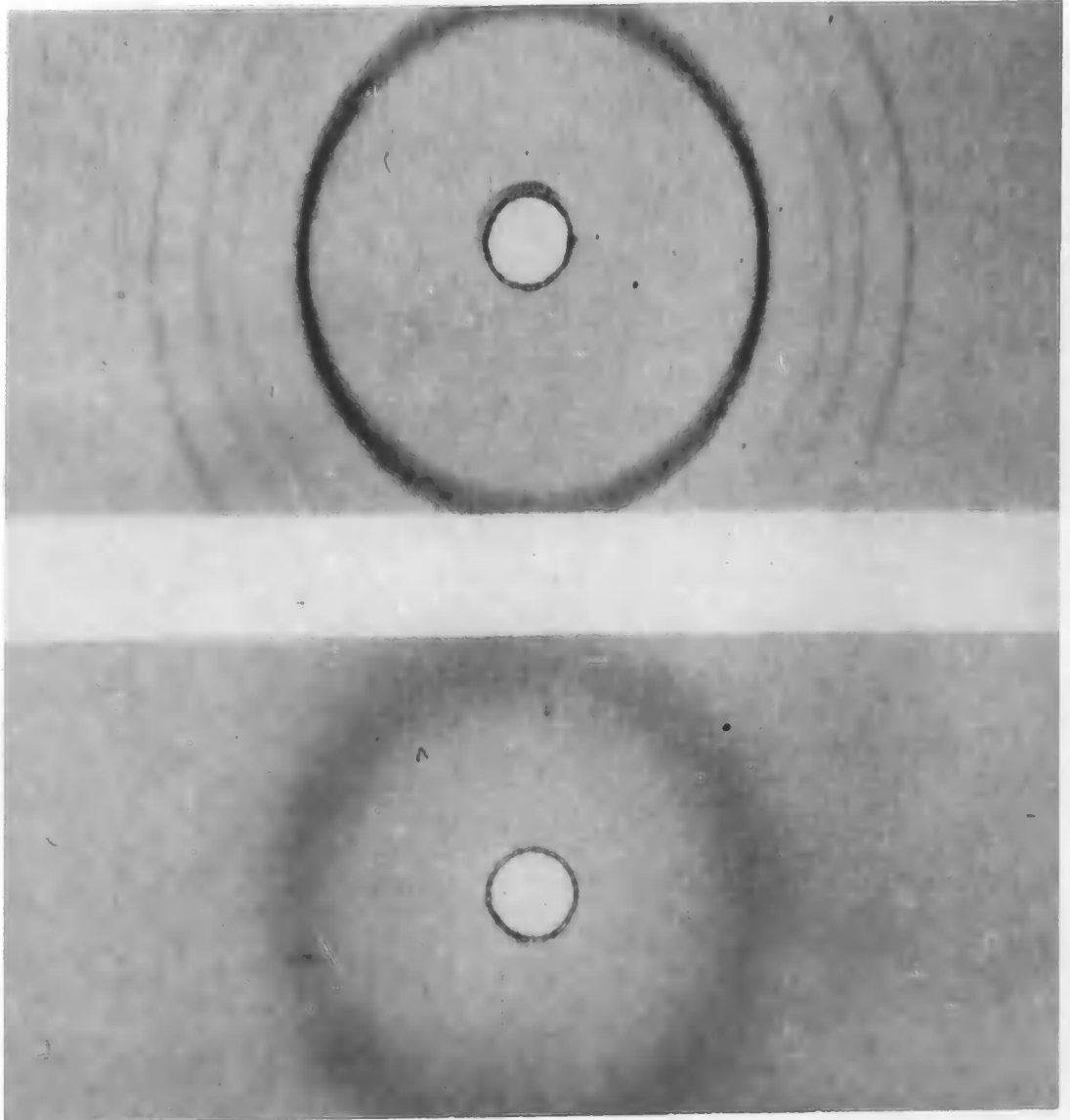
(b) VITREOUS SILICA.

X-RAY DIFFRACTION PATTERNS.

FIG. 1.2

suggested that within the random network one would expect the cristobalite configuration to exist for short distances as one of the varieties of configuration present. The overall picture would be one of small distorted crystals separated by large zones of less order. The observed similarity between the X-ray diffraction patterns of cristobalite and vitreous silica was thus explained.

The first experimental evidence in favour of Zachariasen's predictions came in 1938 when Warren and Biscoe (5) calculated the bond lengths in silicate glasses. The figures obtained indicated a packing consistent with a random network. The work of Warren and Biscoe is outlined, in some detail, in the X-ray section.

There has grown up and still exists a considerable controversy in the literature concerning the basic nature of glass. Even the structure of pure vitreous silica is not yet completely determined (6), and this substance is uncomplicated as glasses go. The facts seem to point to the conclusion, however, that while many industrial advances in glass technology have been made (7) from purely empirical cut-and-try methods, the present picture of glass structure at the atomic level is only now beginning to emerge. This is because, at long last, more powerful physical methods are being used to study glass systems.

1.2 Glass-Ceramics.

A new field of glass technology, namely the conversion of glass to fine-grained crystalline "glass-ceramics", was first announced by Corning Glass Works in 1957. This development was made possible by the discovery of methods of catalysis, or heterogeneous nucleation, whereby crystal growth starts simultaneously from many nuclei dispersed throughout the glass, after the glass article has been formed.

An ideal technique for producing a uniformly fine grained crystalline article from glass involves first introducing submicroscopic catalyst crystals in a high degree of dispersion at a temperature below the range in which the crystals of the major phases can grow at an appreciable rate.

Fortunately, this is easily accomplished in many glasses by dissolving in the molten glass a minor ingredient, the catalyst or nucleating agent, and cooling the glass until the catalyst is homogeneously nucleated and precipitates spontaneously in submicroscopic particles throughout the glass. The glass is then reheated to a temperature and for a time that permits heterogeneous nucleation and growth of crystals, initiated by the catalyst particles. This homogeneous nucleation is obviously inhibited in the normal

melt.

A lithium aluminosilicate material nucleated by the addition of titania is now marketed under the trade name "Pyrosil" by George Jobling & Son of Sunderland.

Pyrosil is capable of withstanding severe thermal shock due to the low thermal expansions of the phases which crystallise. The major crystalline phase present is either beta-eucryptite or beta-spodumene depending on the heat treatment. Both these metastable solid solution phases are closely related to crystalline forms of silica and exhibit a negative volume thermal expansion coefficient over a wide range of temperature when stabilised by lithium ions. Neutrality is achieved by the controlled substitution of aluminium ions for silicon in the tetrahedra. These attractive thermal properties allied with the good mechanical and impact strength of ceramic ware, have been exploited in the manufacture of domestic ovenware as well as many industrial applications.

The physical, chemical, optical and electrical characteristics of glass-ceramics vary far more with chemical composition than do those of glasses so that it is difficult to generalize on this subject. Glass-ceramics usually have an opaque glossy appearance, either white or coloured, although some compositions may also be transparent.

The hardness and scratch resistance of many glass-ceramics are greater than those of glasses or most conventional ceramics. In addition to this, these materials possess desirable wear characteristics for applications such as high temperature bearings since they wear smoothly and uniformly, maintaining a polished surface.

Glass-ceramics maintain their rigidity to higher temperatures than any conventional glass because of their crystalline structure. Some have softening temperatures of $1250^{o}C$ and higher. As previously mentioned, thermal expansion coefficients range from negative values through zero to over 200 x $10^{-7}/^{o}C$, depending on chemical composition and crystal structure. The glass-ceramics having thermal expansions near zero are practically immune to breakage by thermal shock.

In electrical properties, most but not all glass-ceramics are classed as electrical insulators, having dielectric constants between 5 and 10, power factors ranging down to extremely low values comparable with the best electrical ceramics, and excellent dielectric strength.

Considering the multiplicity of materials which have been, and continue to be, developed in recent years, it is difficult to put any one material into its proper perspective or evaluate its future contribution. Nevertheless

one is aware of potentialities in the glass-ceramic field

which remain to be discovered and exploited.

1.3   In the past, most glass studies have been concerned

with bulk properties such as viscosity, density, specific

heat, thermal conductivity and expansion, hardness, strength,

optical transmission, and electrical conductivity and

dielectric properties.

The newer physical methods which can be used to probe

the basic structure of glasses are X-ray and neutron

diffraction, infra-red and optical spectroscopy, electron

microscopy, Mössbauer effect, nuclear and electron

paramagnetic resonance. No one of these methods tells the

whole story or even a large part of it. Whereas, for example,

X-ray analysis will usually completely determine the structure

of a single crystal, only very broad, hard to interpret

spectra result when this method is used on glasses. The most

fruitful approach, then, is to study a glass system with as

many different techniques as can be applied, and attempt to

infer glass structure from the results of these investigations.

As a preliminary to an extended study of the nucleated

crystallisation process, it was the purpose of the work

described in this thesis to look for properties which are

sensitive to a crystalline environment about the constituent

end a variety of techniques have been employed in an examination of the physical properties of soda lime glasses doped with the elements of the rare earth series.

The techniques used were:

(i)   · X-Ray Diffraction Spectra;

(ii)   Conductivity (ionic) Measurements;

(iii)   Magnetic Susceptibility Measurements;

(iv)   Optical Absorption Spectra;

(v)   Electron Spin Resonance.

It was envisaged that;

(i)   would detect any modification to the glass structure brought about by the included rare earth ions and thereby determine the nature of the prepared specimens to be used in subsequent measurements;

(ii)'   would reveal factors introduced into the conductivity of glass by the addition of various ions;

(iv) & (v)   would provide information about the glass matrix which could be used to calculate theoretical values of susceptibility for comparison with the results given by (iii).

CHAPTER TWO.

SPECIMEN PREPARATION.

Unused commercial soda glass tube was finely ground

and the chemical composition established as being 71% SiO_2

17% Na_2O and virtually free from iron impurity. (A complete

analysis is given in Appendix I). Additions of rare earth

oxides to this finely ground base glass were made on a

weight basis and the components ground together in an agate

mortar in an attempt to achieve homogeneity. Each mix was

carefully transferred to a quartz glass thimble capable

of holding about ten grammes. Quartz glass was chosen for

its high melting point and corrosion resistance.

Melting was done in a Crusilite rod box furnace fitted

with an electronic indicating pyrometer controller and

energy regulator. Consequently, heating to or cooling from

the maximum temperature of $1300°C$ could be precisely

controlled.

A typical melting cycle would be:

(i)   A rise to $700°C$ over four hours. This allows

the entrapped air to expand and escape gradually

without blowing the mix out of the thimble.

(ii)   The furnace temperature was then raised to

$1300°C$ by which time the soda glass is fluid. It was

then left at this temperature for three hours to allow

included air bubbles to rise to the surface.

(iii) After cooling to 600°C, at a rate of 200°C per hour, the furnace was held at this annealing temperature overnight.

(iv) Cooling to room temperature was achieved by switching off the furnace, the insulation being so effective this took a further four hours.

The specimen was easily separated from the now devitrified quartz glass thimble.

By this method the following specimens were prepared for examination:

(i)   Soda Glass standard;

(ii)   5% Praseodymium Oxide

(iii) 5% Samarium Oxide

(iv)   1%
       5%
       10% Gadolinium Oxide   (by weight)
       20%   in
       30%   Soda Glass.

(v)   5% Dysprosium Oxide

(vi)   5% Erbium Oxide

With the exception of the 20% and 30% gadolinium oxide

additions, the oxide was completely dissolved in the soda glass. The resulting specimen was transparent although, in some cases, the rare earth ion caused colouration. The soda glass would not take up the higher percentages of gadolinium oxide, the result being an inhomogeneous mixture of glass and powder.

CHAPTER THREE.

X-RAY SPECTRA.

3.1 Introduction.

The X-ray diffraction pattern of a glass consists of one or more broad diffuse rings. It is distinctly different from the powder pattern of a crystalline material, which shows a large number of fairly well defined rings. The X-ray diffraction patterns of vitreous silica and crystalline silica (cristobalite) have been shown in Figure 1.2. Microphotometer records of the diffuse patterns can be plotted as intensity curves (Figure 3.1a) and, in turn, radial distribution curves obtained, by Fourier analysis, from the intensity curves (Figure 3.1b).

Each distribution curve is the sum of four distribution curves, namely, the atoms about a silicon, an oxygen, a calcium and a sodium. The position of a peak in a curve of Figure 3.1b therefore gives the distance between a pair of atoms, provided the various interatomic distances are sufficiently different from one another so that the corresponding peaks are resolved.

Using this method J. Biscoe (8) concluded that the Si - O distance is $1.62\overset{\text{o}}{\text{A}}$ and, by calculating the area

RADIAL DISTRIBUTION CURVES OF
SODA-LIME-SILICA GLASSES. (BISCOE).
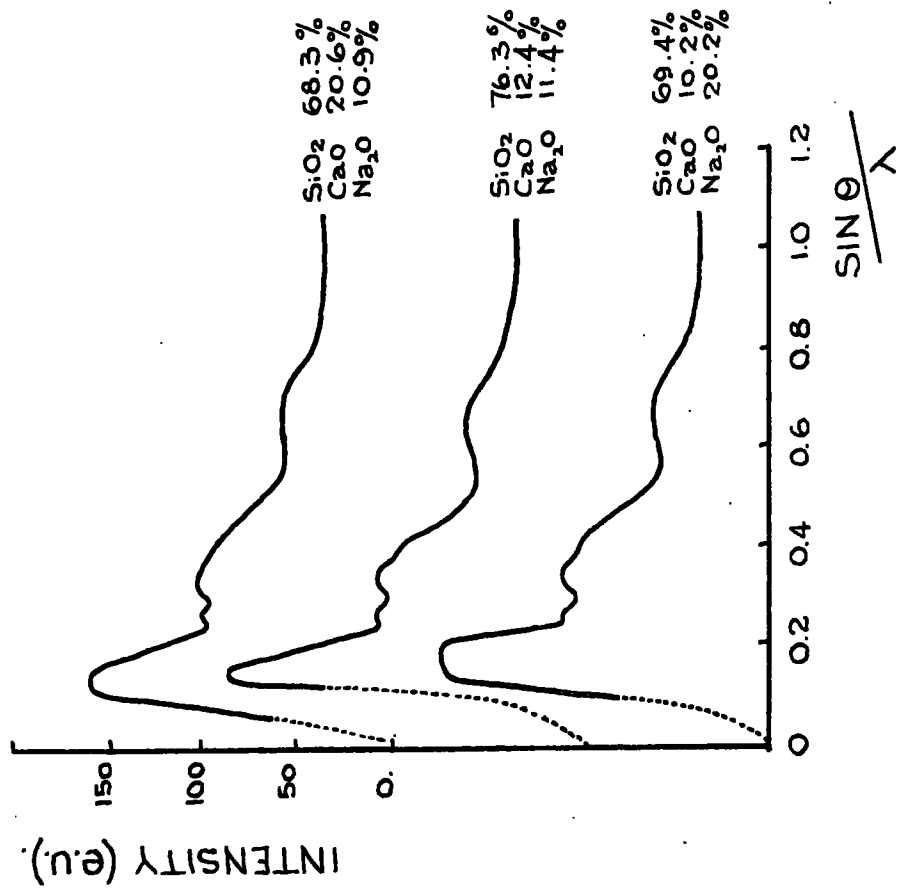
FIG. 3.1b

EXPERIMENTAL INTENSITY CURVES OF
SODA-LIME-SILICA GLASSES. (BISCOE)

FIG. 3.1a

under the peak, that each silicon is surrounded on the average by four oxygens. Furthermore, despite the uncertainty of the peak position, he was able to estimate the inter-atomic distances for the constituents of soda-lime-silica glass as follows:

$$Si - O \qquad 1.62\overset{o}{A}$$

$$O - O \qquad 2.65\overset{o}{A}$$

$$Na - O \qquad 2.35\overset{o}{A}$$

$$Si - Si \qquad 3.20\overset{o}{A}$$

The structure of soda-lime-silica glass, Biscoe suggested, is a three-dimensional random network in which each silicon is surrounded by four oxygens, each approximately at the corner of a tetrahedron. Some of the oxygens are bonded to two silicons and some to one silicon. There are holes in this random network in which the sodium and calcium atoms lie surrounded by six or seven oxygens respectively.

3.2 Experimental Method.

Powder diffraction photographs were taken of each specimen using a Philips 11cm. Debye-Scherrer camera. A $2\frac{1}{2}$ hour exposure to the Co $K\alpha$ source was allowed throughout the series.

3.3 Results.

It was impossible to differentiate between the diffraction patterns produced by the various specimens.

The broad diffuse ring of the specimen containing 10%
gadolinium oxide, shown in Figure 3.2, is typical of the
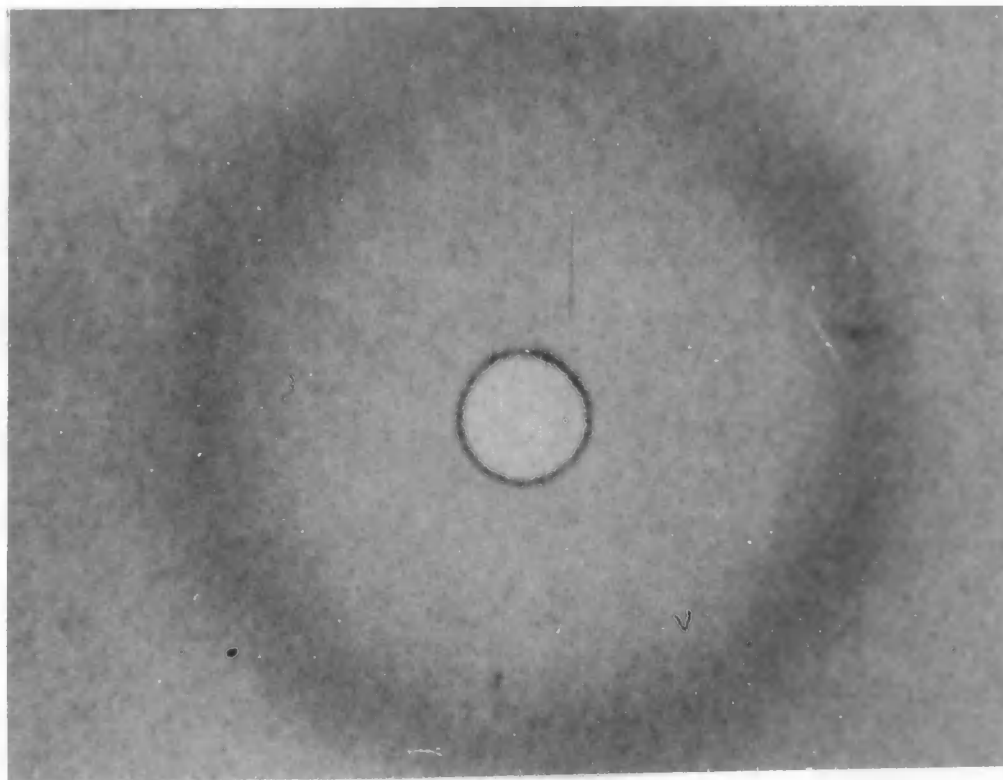specimens examined.

FIG. 3.2.

This result confirms that no crystallisation occurred
during the specimen preparation and that, in subsequent
experiments, one is dealing with a vitreous solid. The
presence of rare earth ions does not appear to modify the
structure but one cannot rule out the possibility of lines
appearing at a large angle.

CHAPTER FOUR.

ELECTRICAL CONDUCTIVITY IN GLASS.

4.1 Glass as an Electrolyte.

The electrolytic nature of glass and in particular the mobility of the sodium ion in soda rich glasses was first demonstrated almost a century ago.

Since that occasion numerous researchers have contributed to the now overwhelming evidence supporting the view that silicates are predominantly ionic conductors. Kraus and Derby (9), for example, electrolysed soda-lime-silica glass between a mercury cathode and a fused silver nitrate anode. A copper voltameter in series measured the current. The sodium electrolysed into the mercury cathode was determined, and also the change in weight of the samples as the silver ions replaced the sodium ions. Furthermore, the depth of penetration of the silver ions could be determined exactly if the glass, after electrolysis was heated sufficiently to precipitate the silver, this treatment producing a deep red-brown colour. These measurements enabled the authors to conclude that the mechanism of conduction was the replacement of one silver ion for each sodium ion as the sodium and silver ions migrated towards the cathode. It was

also concluded that not all the sodium ions were replaced, the percentage which migrated varying progressively from 74.4% to 81.0% as the temperature varied between 278°C and 343°C.

Further evidence of ionic conduction has more recently been given by Peyches (10). A soda glass was irradiated so that part of the sodium became radioactive sodium 24. This glass was placed between electrodes of sodium nitrate at 320°C. The radio-sodium was all found in the cathode bath after a voltage had been applied for sufficient time. The glass appeared to be unchanged otherwise. Peyches concluded that conduction is essentially ionic and, since anions are not observed to move, cations must be the charge-carrying entity.

The electrical conductivity observed in "pure" silica (SiO_2) arises from the presence of current carrying impurities in extremely small concentrations.

The structure of glass is consistent with ionic mobility. The glassy network of silicon-oxygen tetrahedra is relatively rigid at low temperatures and the modifying alkali or metallic ions reside in large cavities as shown in Figure 4.1. They are loosely bonded to the network. The energy barriers that they must pass to move to a nearby cavity are sufficiently low, at least for many cavities,

THE RELATION BETWEEN TIME OF ANNEALING AND THE ELECTRICAL RESISTANCE.
(REBBECK ET AL 29)
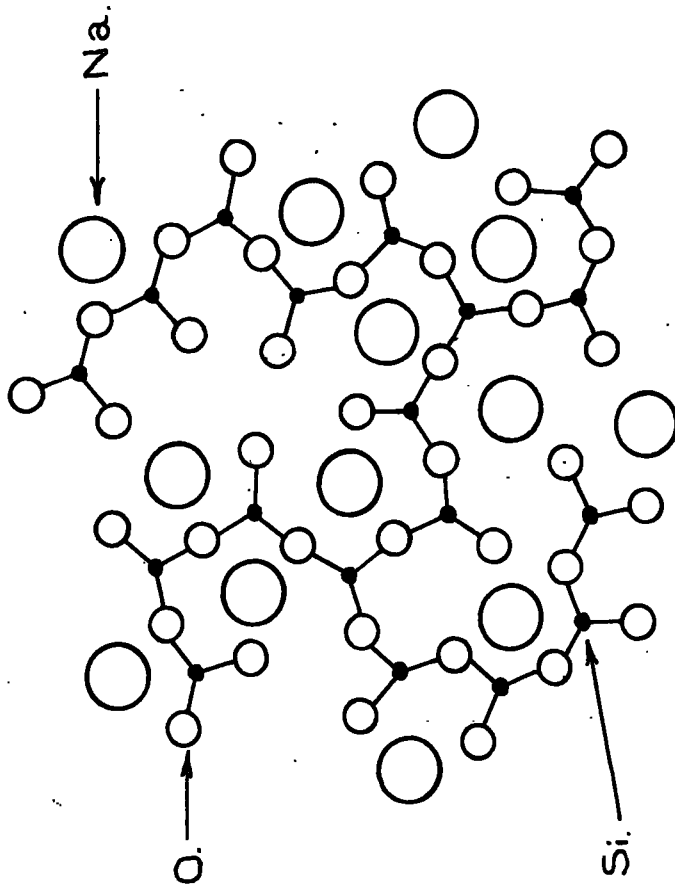
FIG. 4.2

SCHEMATIC REPRESENTATION IN TWO DIMENSIONS OF THE STRUCTURE OF SODA-SILICA GLASS.
(STANWORTH 28).

FIG. 4.1

that a statistical drift of these ions occurs through the glass when the glass is in an electric field. The ability of an ion to migrate through the network will depend basically upon two factors:

(i)   the strength of its holding bond in the lattice;

(ii) its physical size relative to cavity size.

The size factor is substantiated by the lower conductivity exhibited by an annealed glass (see Figure 4.2). The unannealed glass has been chilled so quickly that an open structure of low density is formed, whereas the annealed glass has had plenty of time to rearrange its structure to a higher density arrangement that more closely approaches thermodynamic equilibrium. The open structure of unannealed glass permits ion motion much more readily and, perhaps, to some extent, permits a larger fraction to participate. The compact annealed structure inhibits ion motion and has a much higher resistance.

One might expect a similar result if, instead of decreasing the cavity size by annealing, large ions were introduced into the network cavities to inhibit the drift of smaller monovalent ions. This was in fact illustrated by Fulda (11) who replaced silica, weight for weight, by other oxides in what was originally a simple soda-silica composition. The data he collected, shown graphically in Figure 4.3, shows
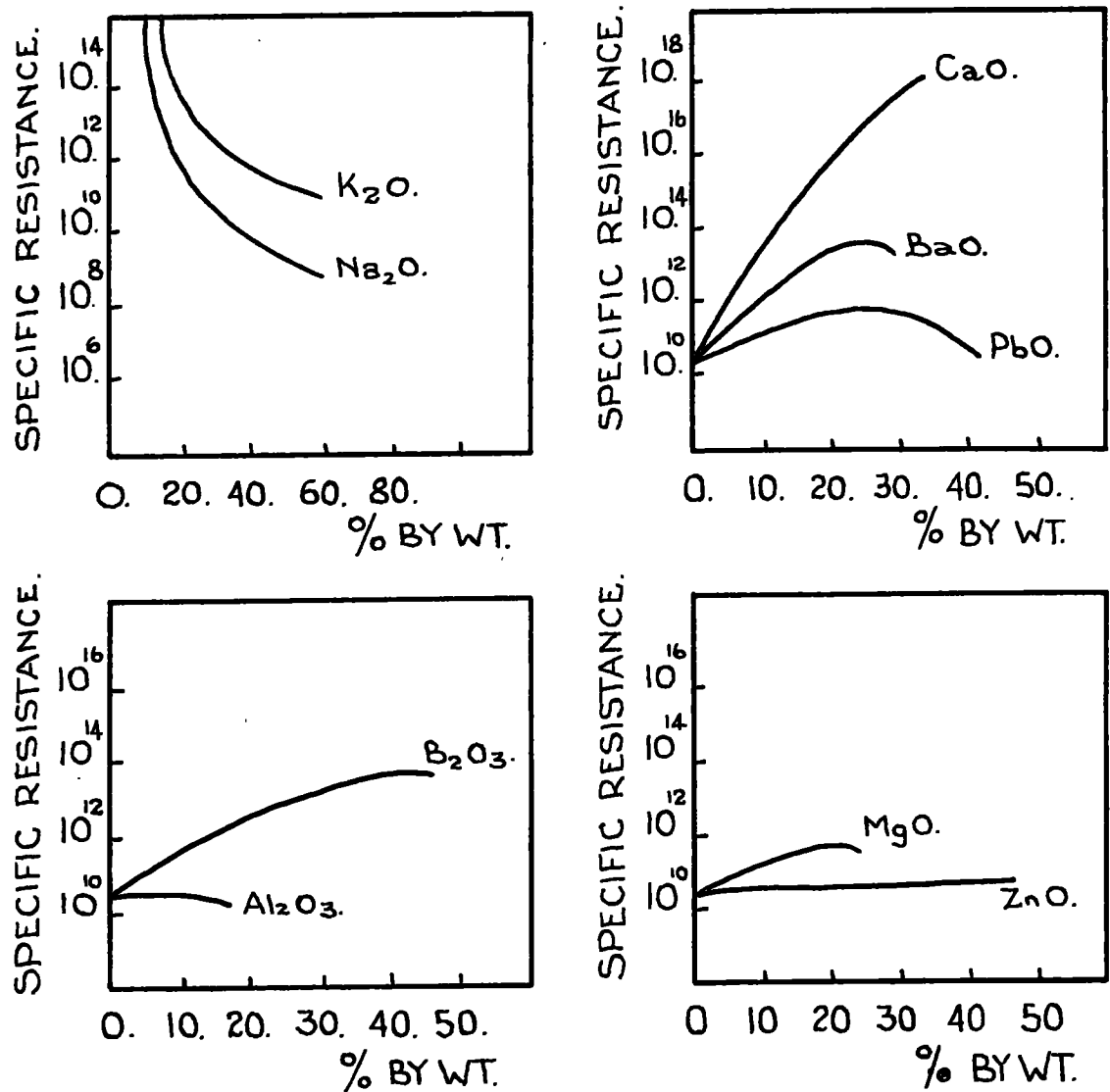
THE EFFECT ON SPECIFIC RESISTANCE OF A GLASS OF THE
COMPOSITION 18% SODA, 82% SILICA, OF REPLACING SILICA
BY THE INDICATED PERCENTAGE BY WEIGHT FOR OTHER OXIDES.
THE GLASS FOR SODA & POTASSIUM OXIDE REPLACEMENT BEGINS
AT 20% LEAD OXIDE, 80% SILICA.   (FULDA)

FIG. 4.3

that the oxides of sodium and potassium raise the conductivity

drastically, as would be expected from the ionic theory of

glass conductivity. Note that potassium oxide is not as

effective as soda, at least on a weight percentage basis,

but both increase conductivity. Conversely, with the exception

of alumina, other oxides tend to decrease the conductivity.

These divalent cations would seem to be bound in such a way

as to block the flow of alkali ions,hence increasing ρ. The

peaks in ρ for certain oxides such as that of barium are

evidence of their loosening effect on the network.

4.2 <u>Dependence of Conductivity on Temperature.</u>

The dependence of conductivity on temperature was

first established by Fousseron in 1882. The rapid decrease

in resistivity (ρ) with increasing temperature is expressed

by Rasch and Hinrichsen's equation (12)

$$\rho = A e^{B/T}$$

where A and B are constants and T is the temperature measured

on the Kelvin scale.

The results obtained by Fulda,shown graphically in

Figure 4.4, would indicate that the equation cannot be

applied through the complete temperature range since the

constants will change at the transition points. Fulda gives

measurements on one glass of the following composition in

per cent, from room temperature to $1200^{\circ}C$: 71 silica;

SPECIFIC RESISTANCE.

$\frac{1}{2}$ DEG. PER MIN.

1 DEG. PER MIN.

5 DEG. PER MIN.

9 DEG. PER MIN.

12   13   14   15   16

$\left(\frac{1}{T}\right) \times 10^4$

EFFECT OF RATE OF TEMPERATURE
INCREASE ON TRANSFORMATION
POINT.   (FULDA)

FIG. 4.5

SPECIFIC RESISTANCE.

10^{12}
10^{11}
10^{10}
10^{9}
10^{8}
10^{7}
10^{6}
10^{5}
10^{4}
10^{3}
10^{2}
10

1200 800 600   400   200   °C.

10 12 14 16 18 20 22 24 26 28

$\left(\frac{1}{T}\right) \times 10^4$

VARIATION OF SPECIFIC RESISTANCE
(LOG. SCALE) WITH RECIPROCAL OF
ABSOLUTE TEMPERATURE.   (FULDA)

FIG. 4.4

5.4 lime; 12.5 soda; 8.7 potassium oxide; 2.4 alumina. The resistance varies linearly with $1/T$ up to a temperature of approximately 460°C where there is a gradual transition to a second straight line ending at about 650°C. From 900°C to 1200°C the resistance changes very slightly. This first transition point is generally referred to as the "transformation point". At this temperature he found the electrical conductivity of strained and annealed glass to become the same. He states that with unstrained glass there is no well-defined break in the curve but only a gradual transition from one direction to the other. By increasing the rate of heating during measurement, the apparent change can be made more marked. Figure 4.5 shows this effect.

The conclusions that must be drawn from Fulda's results are that:

(i)   there is no sudden discontinuity in the electrical conductivity of annealed glass, but a slow change, the rate of which probably depends upon the viscosity of the glass . The change lags behind the temperature for the more rapid changes and, when it does begin, it operates so as to give the appearance of a critical temperature point.

(ii)   the log ρ v $1/T$ graph is by no means a straight line which would indicate either the failure of

the Rasch-Hindrichsen equation or that A and B

are temperature dependent. The latter is true for

most glasses and generally two values of A and B

are sufficient to define ρ . The exceptions,

particularly in the molten state, have an

activation energy markedly dependent upon

temperature and obey the equation

$$\log \rho = A' + B'T$$

Since all glasses in the vitreous state and most

glasses in the molten state obey the Rasch-

Hindrichsen equation it is regarded as the

fundamental equation giving a description of

the conductivity of glass in general. ·

The temperature dependence of resistance has been

acknowledged in the manufacturing process for many years

where the preliminary heating is done by conventional

burners until the furnace charge becomes sufficiently

conductive to use electric current for local heating.

4.3 Measurement of Conductivity in Glass.

In deciding which method to employ for the conductivity

measurements one must consider the inaccuracies inherent in

the alternatives. Alternating current methods, for example,

give rise to A.C. losses which can cause the measured

conductivities to be higher than the true D.C. values. Direct

current methods, on the other hand, are subject to errors arising from the decay in the magnitude of the current-carrying alkali ions near the negative electrode. Since the data obtained was intended to show comparative conductivities rather than absolute values, an A.C. bridge method was selected on the basis of sensitivity and flexibility.

4.4 The A.C. Bridge.

The selection of a suitable A.C. bridge for the investigation was based upon the assumption that the equivalent parallel resistance and capacitance values of the specimen's impedance would be in the order of 10^{14} ohms and 1pF respectively and that it would be necessary to detect changes of at least 0.5 per cent. of these values. As the measurements were to be made with the temperature continuously varying, it was also necessary to use a bridge in which the balance point could be quickly found. The method which is normally used to satisfy these standards of accuracy is the Schering bridge. Unfortunately, the balance point of the bridge is affected by stray capacities to earth and a Wagner zero must be obtained before each observation. Consequently, the time required for each reading is longer than desirable thereby eliminating this bridge for the measurements.

In 1928 Blumlein (13) proposed an alternative scheme

to reduce earth capacitance effects. This involved replacing the usual resistive ratio arms by a pair of tightly coupled inductors, earthed at their common point, whose turns ratio would be equal to their impedance ratios. The principle and practice of a variety of inductively coupled ratio arm bridges was outlined by Clark and Vanderlyn in 1949 (14).

The bridge circuit is shown in Figure 4.6. T_1 is the coupling transformer and T_2 the ratio arm transformer. R_1 and C_1 balance the resistive and capacitative components of the specimen impedance shown as a parallel arrangement of R and C. R_2 and R_3 are resistance range selectors.

With the notation of Figure 4.6, the balance condition for this bridge is

$$\frac{n_1}{n_2} = \frac{C}{C_1} = \frac{R_1R_2 + R_2R_3 + RR_3 + RR_1}{RR_2}$$

as derived in appendix II

In the construction of this bridge the internal and external connections were made with screened lead. The ratio arm transformer, T_2, was hand wound onto a ferrite core; the effective turns ratio being adjusted to $n_1/n_2 = 1/100$. This was done by comparing the signal amplitudes on a cathode ray oscilloscope.

The resistance balance arm, R_1, consisted of five decade boxes of selected carbon composition resistors and

T₁

T₂

L₁   L₂

DETECTOR.

C₁   C
                            R

R₃

R₁   R₂
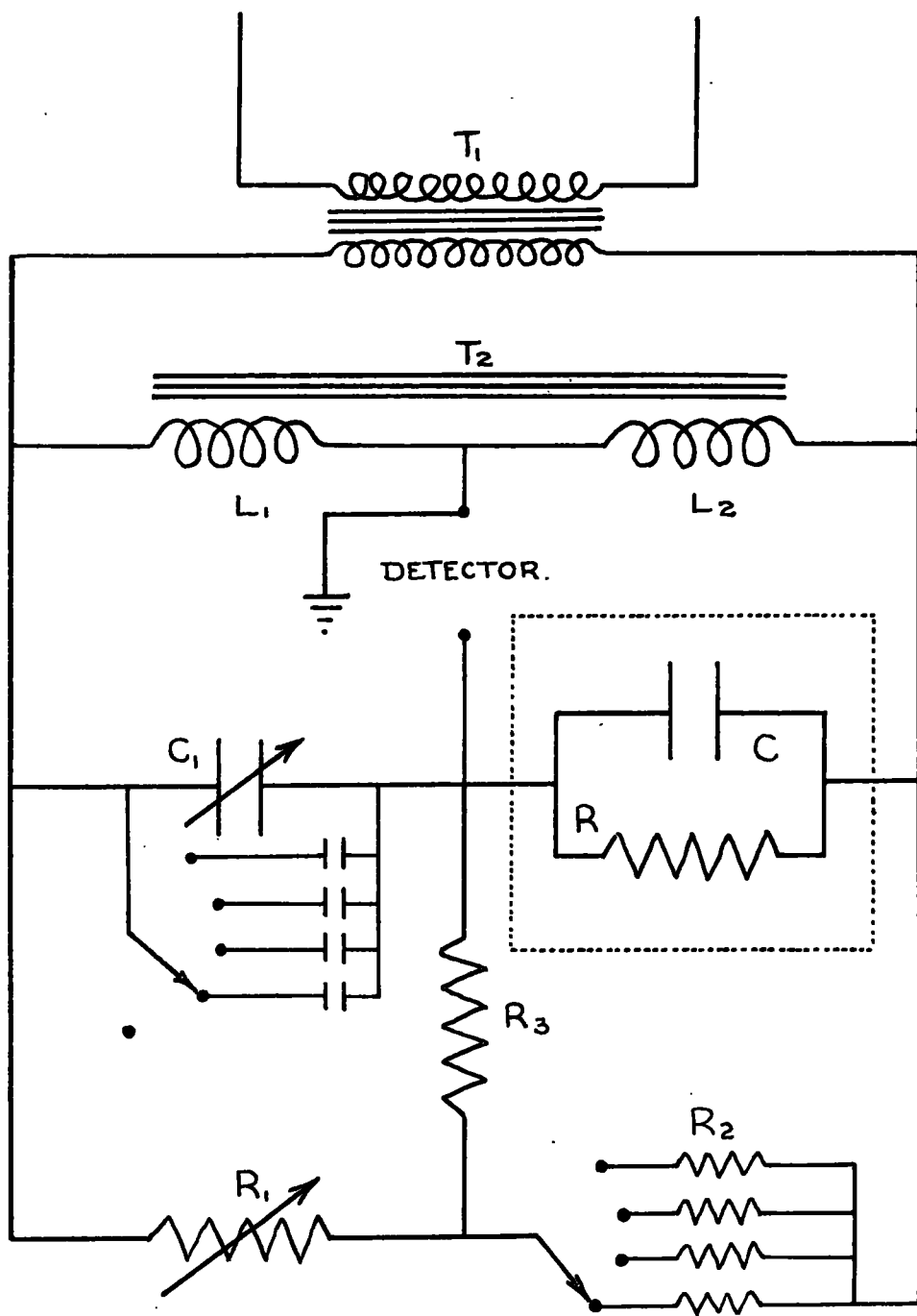
THE A.C. BRIDGE CIRCUIT.

FIG. 4.6

a 100 ohm potentiometer. This gave R_1 possible values ranging from 0 to 10^7 ohms, if necessary, in one ohm steps. Calibration of the bridge was achieved by measuring known resistance values. A typical calibration curve is shown in Figure 4.7. Defining sensitivity as $\Delta R_1/\Delta R$ it will be seen that as R increases sensitivity decreases. Readings on the most sensitive, linear portion of the calibration curve are hampered by very small currents and it was preferable to function on the middle region sacrificing some sensitivity for a more detectable current. It will also be noticed that there is a lower limit to the resistance that can be measured.

By increasing the value of the fixed resistance, R_3, the calibration curve is moved to higher R values. This increases the accuracy of measuring high resistances and also raises the minimum value. Values of R_2 and R_3, in the ratio R_3/R_2 : 2/1, were selected by a wafer switch giving five resistance ranges capable of measuring R values from 10^6 to 10^{14} ohms within the prescribed limits of accuracy. A separate calibration curve was necessary for each of the five ranges. Since the frequency dependence of the bridge resistors introduced a progressive error into the use of the calibration curves it was decided to calibrate and operate the bridge at 900 Hz.

The standard capacity, C_1, was an 80 pF air spaced

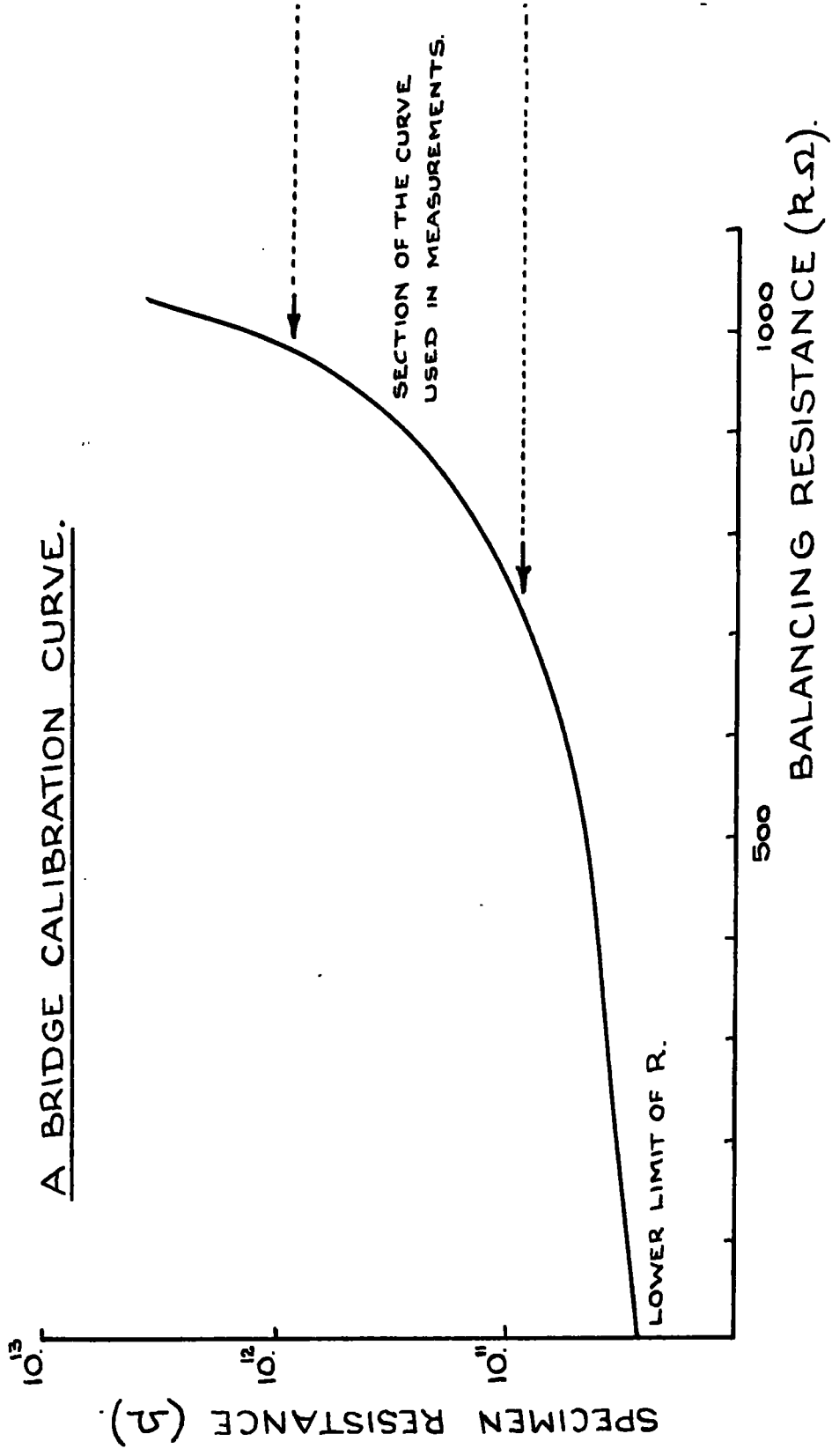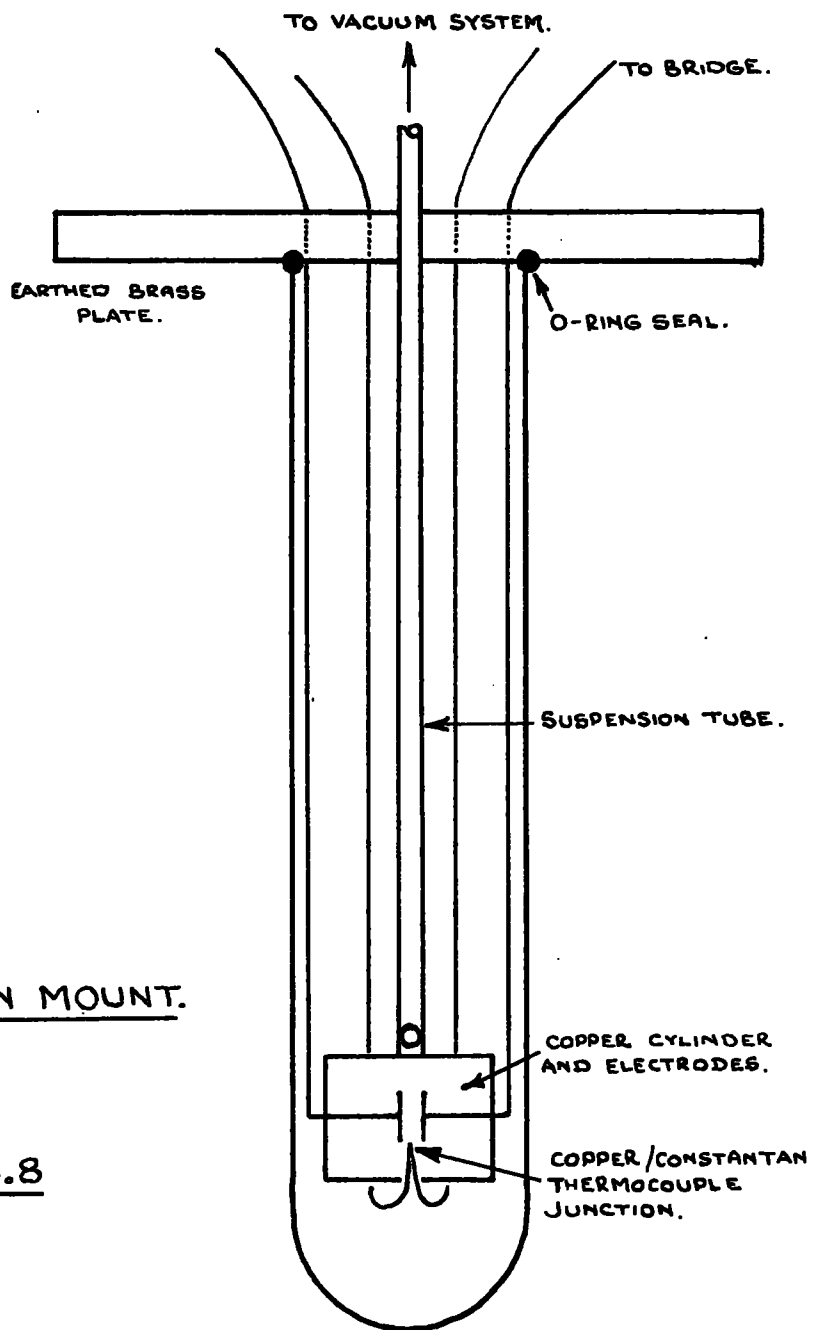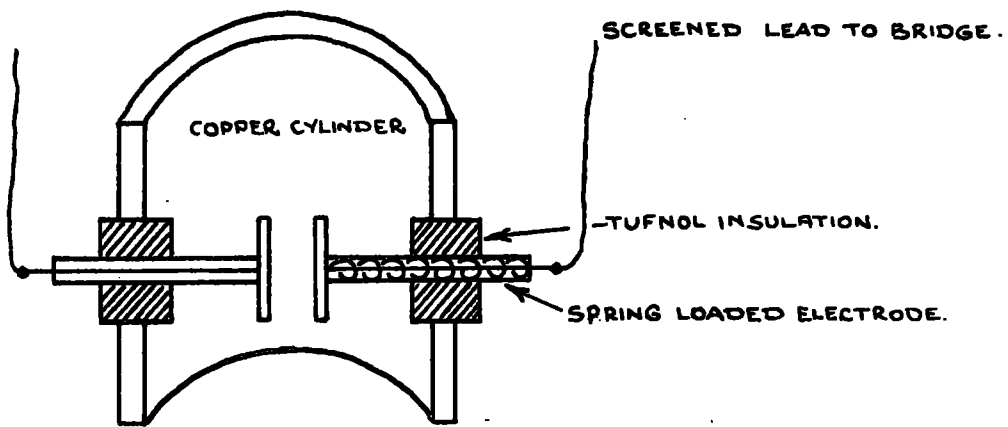A BRIDGE CALIBRATION CURVE.

FIG. 4.7

capacitor with a minimum value of 20 pF. Fitted with a slow motion drive it was possible to obtain changes of 0.2 pF, which of course means a detectable change of 0.002 pF in a specimen of capacity 0.2 to 0.8 pF. For capacities greater than 0.8 pF provision was made to switch standard capacitors in parallel with the variable capacitor.

A Farnell low frequency oscillator was used as the source and a Dymar A.F. wave analyser as the null point detector.

4.5   The Specimen Mount.

The specimen mount is shown in Figure 4.8. The two spring loaded brass electrodes were insulated from the rest of the mount by cylinders of tufnol several times thicker than the glass specimen to be measured. This minimised the chance of an unwanted conduction path appearing.

The specimen was effectively held at the centre of a cylindrical copper box, one end of which was threaded for easy access. Although this removable cap was drilled to allow circulation, the whole formed an excellent low temperature enclosure and radiation shield. This holder was suspended from an earthed brass plate by a stainless steel tube, the latter passing through the plate and being hard soldered into place. The plate had an O-ring groove such that the suspended holder could be encased in a vacuum tight glass

SCREENED LEAD TO BRIDGE.

COPPER CYLINDER

TUFNOL INSULATION.

SPRING LOADED ELECTRODE.

TO VACUUM SYSTEM.

TO BRIDGE.

EARTHED BRASS PLATE.

O-RING SEAL.

SUSPENSION TUBE.

THE SPECIMEN MOUNT.

COPPER CYLINDER AND ELECTRODES.

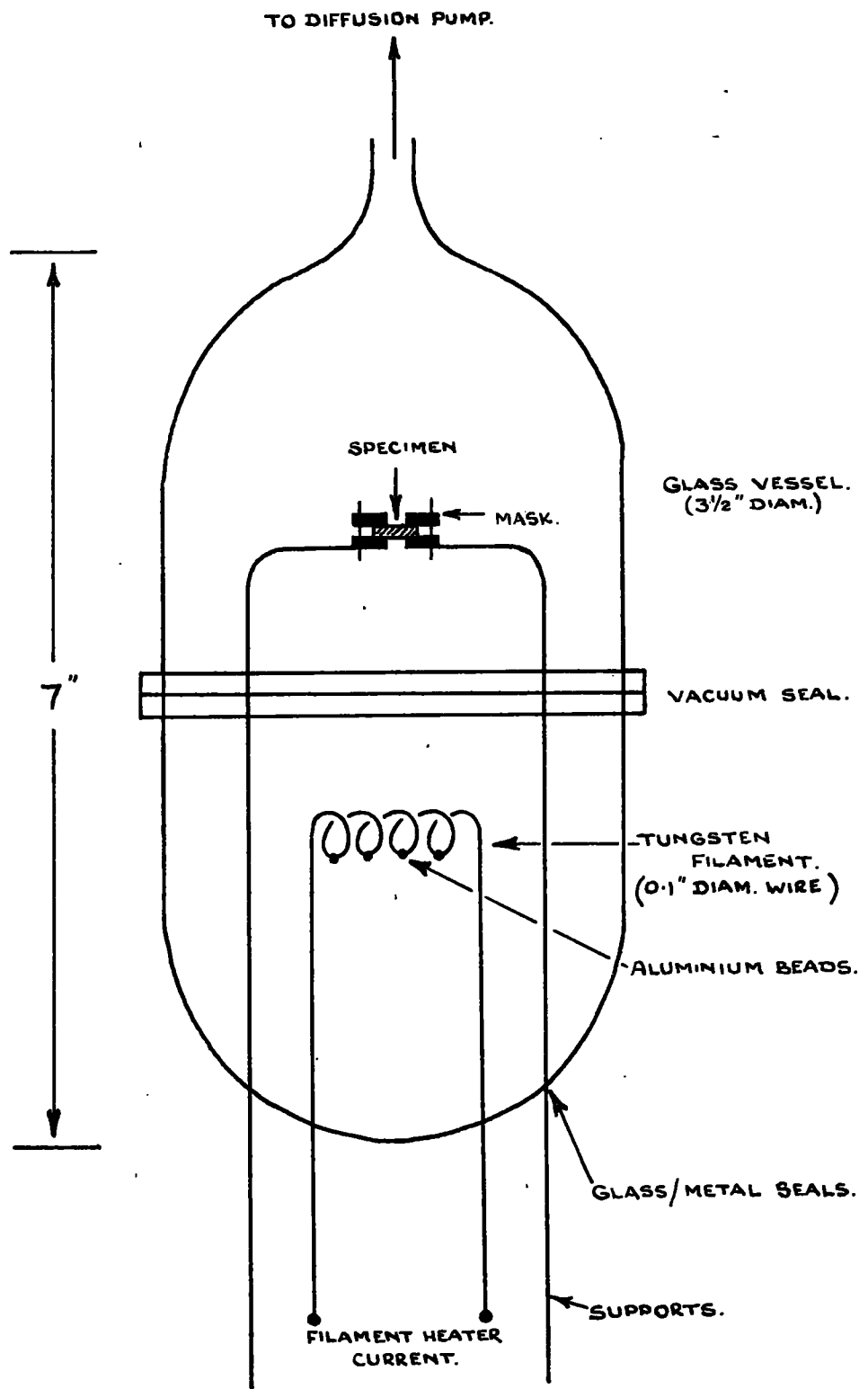COPPER/CONSTANTAN THERMOCOUPLE JUNCTION.

FIG. 4.8

tube. When not under vacuum the tube was held in position by springs. Access for electrical connections and thermocouple wires was via lead-throughs soldered into the brass plate. Specimen temperature was measured by a copper/constantan thermocouple junction situated inside the copper holder. The specimens were cut from the prepared rare earth doped glasses to the specification $1/8''$ x $1/8''$ x $3/64''$ thick.

As regards a satisfactory electrical contact with the specimen, two methods were investigated.

(i) <u>Evaporated Aluminium Contacts.</u>

A diagram of the evaporation vessel is given in Figure 4.9. The glass evaporation vessel was made in two sections. Glass/metal seals provided vacuum tight access for four $1/32''$ diameter rods, two of which supported the specimen and the other two the tungsten wire filament. With the sections in vacuum tight contact the vessel was evacuated to a pressure of 10^{-6} millimetres of mercury. The filament current was then gradually increased until the aluminium foil beads on the now white hot filament melted to form globules. A further small increase in current caused a rapid evaporation of the molten aluminium. This stage was characterised by the silvering of the glass vessel in the vicinity of the outlet to the diffusion pump. The specimen was masked such that the aluminium vapour condensed to form a conducting spot, about $3/32''$ in

TO DIFFUSION PUMP.

SPECIMEN

GLASS VESSEL.
(3½" DIAM.)

MASK.

7"

VACUUM SEAL.

TUNGSTEN
FILAMENT.
(0·1" DIAM. WIRE)

ALUMINIUM BEADS.

GLASS/METAL SEALS.

SUPPORTS.

FILAMENT HEATER
CURRENT.

THE EVAPORATION VESSEL.

FIG. 4.9

diameter, on its surface.

(ii) <u>Aluminium Foil Contacts.</u>

Aluminium foil discs, $^1/8"$ in diameter, were held in contact with the specimen by the spring loaded electrodes.

Measurements were made on a specimen fitted with aluminium foil contacts. Aluminium contacts were then evaporated onto this same specimen and the measurements repeated. There was no noticable difference between the data obtained in each case. Therefore, being the simpler method, foil contacts were used throughout the series.

4.6. <u>Experimental Method.</u>

Even though the specimens were stored in a dehydrating environment it was deemed necessary to take precautions against surface moisture before each series of measurements. This was done with the specimen in situ by warming under vacuum and finally flushing with dry helium gas. The presence of the helium gas had two important functions:

(i) to ensure efficient heat exchange between the copper enclosure and the surrounding medium;

(ii) to prevent condensation at low temperatures.

To minimise the temperature differential between the specimen and the thermocouple junction, due to their vastly different heat capacities, a small glass bead was placed over the junction and temperature variations made as gradual

as possible (in the order of 5 deg.min^{-1}). Measurements

below room temperature were obtained by gradually immersing

the glass tube surrounding the specimen mount in liquid

nitrogen. The temperature fell at the prescribed rate to a

minimum value of 87°K. At this point the cooling medium

was gradually removed and the measurements repeated as the

specimen warmed to room temperature. The coolant was replaced

by a container of Lissapol which was warmed from room

temperature to 460°K, the boiling point of Lissapol, by a

small bunsen burner flame. Measurements, made during this

temperature rise, were repeated as the specimen cooled to

room temperature. The results were the same for both the

heating and cooling run.

4.7 Results.

The experimental data obtained is shown graphically

in Figure 4.10 through to Figure 4.17. In each case it is

presented in the form specific resistance, on a logarithmic

scale, against the reciprocal of absolute temperature. From

these curves it is clear that, for all the specimens

examined, the specific resistance is accurately given by

the law

$$\rho = A e^{B/T}$$

It will be noticed however that in every instance the

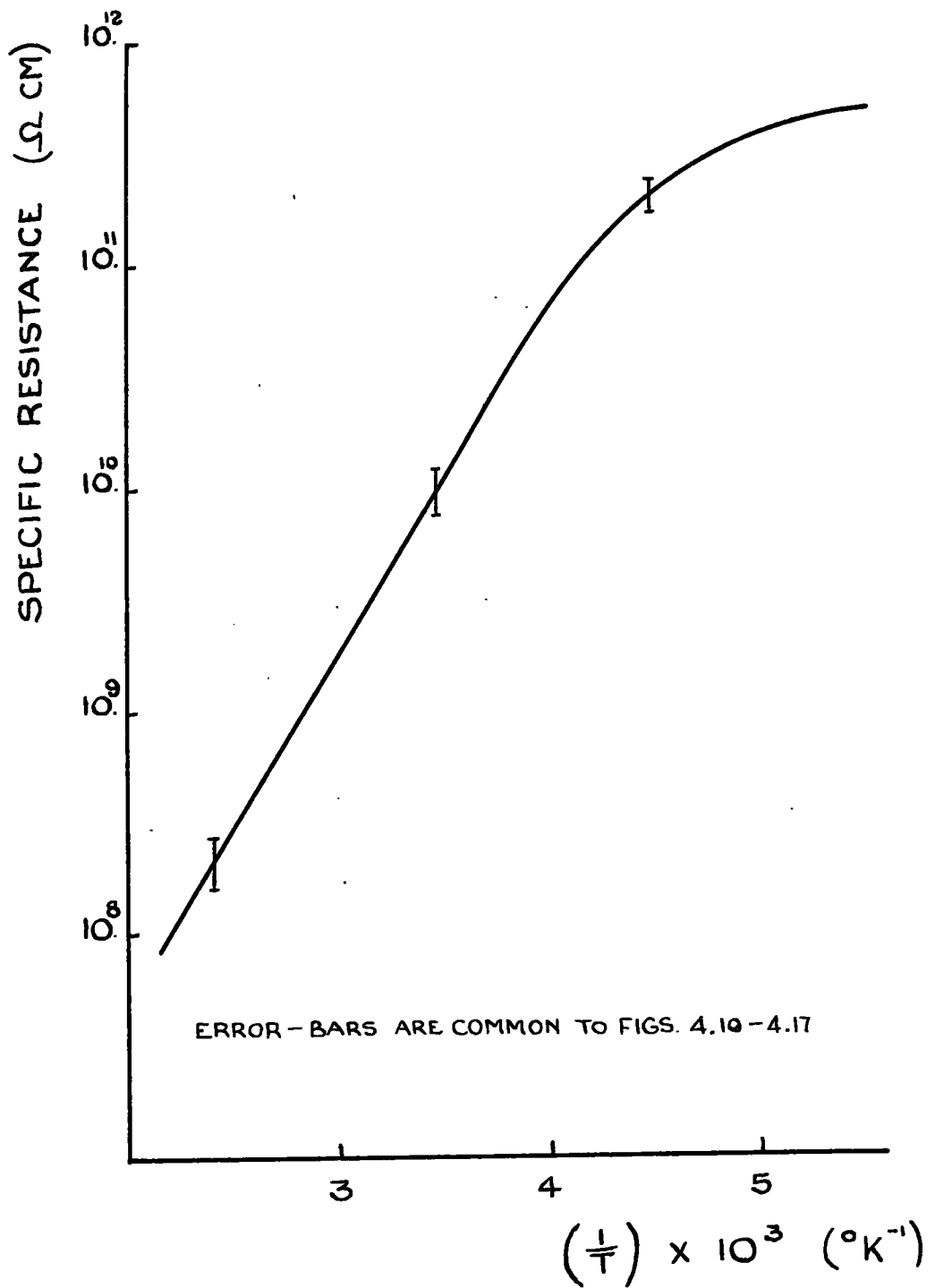gradient decreases when the specific resistance reaches a

value of 2×10^{11} ohms. This is interpreted as the formation

of an alternative conduction path. As the specimen resistance

increases it will eventually become comparable with that of

the insulation in the holder and the latter becomes

significant in a role of parallel resistor. The resistance

relationship beyond this point is not representative of the

specimen alone.

The variation of the activation energy, A and

are shown in Table 4.1.

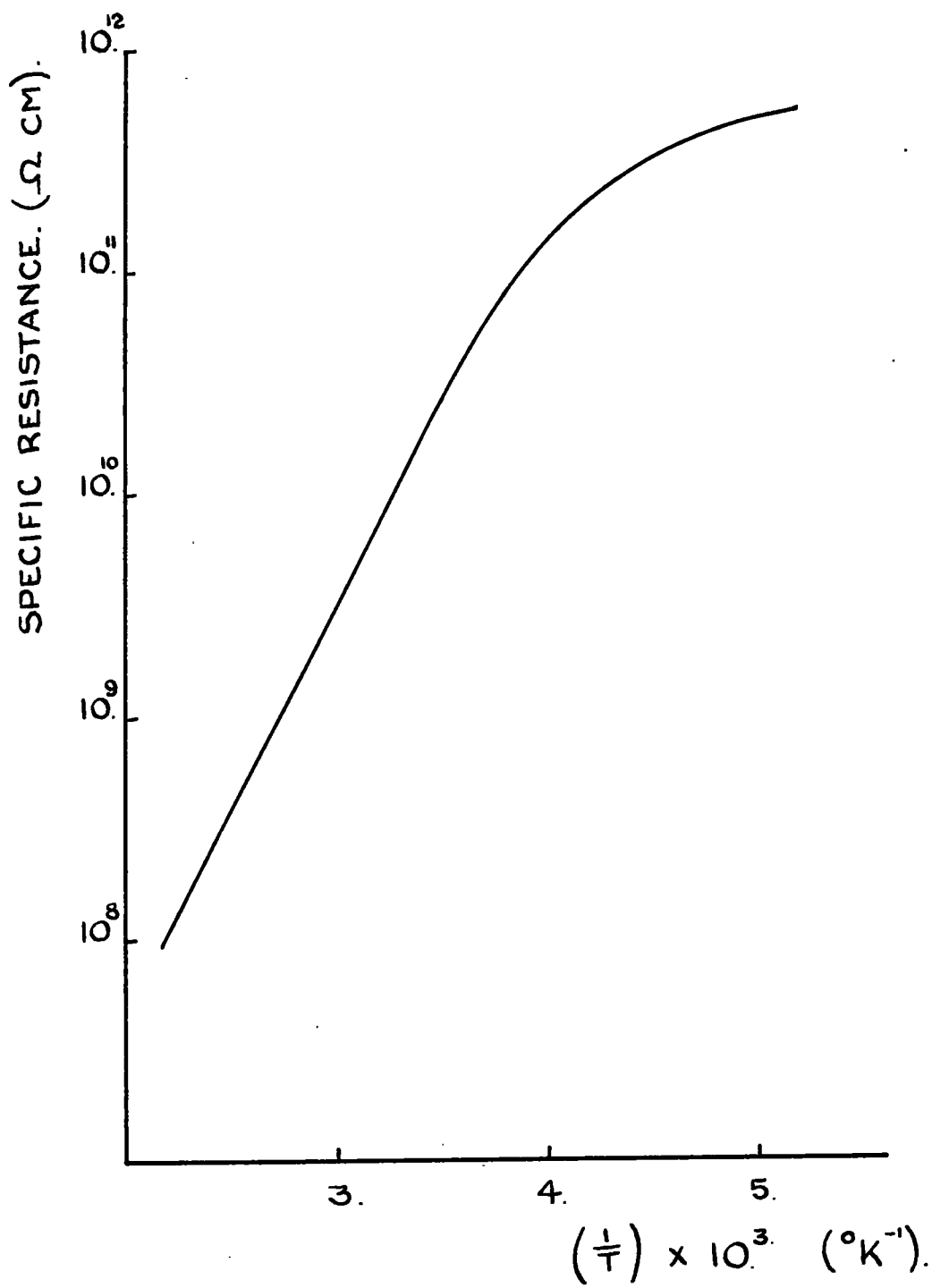| Ion Implanted	Activation Energy (eV)	A (Ω cm)	ρ_{300} (Ω cm)
Soda Glass Standard	0.31	4.0×10^4	6.3×10^9
Pr^{3+}	0.39	6.3×10^3	1.2×10^{10}
Na^{3+}	0.43	6.3×10^2	1.1×10^{10}
Sm^{3+}	0.33	3.0×10^4	8.0×10^9
Gd^{3+}	0.42	2.1×10^3	1.4×10^{10}
Gd^{3+} (10%)	0.43	1.1×10^3	1.1×10^{10}
Dy^{3+}	0.41	2.4×10^3	1.4×10^{10}
Er^{3+}	0.23	3.3×10^5	2.3×10^9

Table 4.1

With the exception of erbium oxide the activation energy is

increased by the addition of rare earth oxides to soda glass.

SPECIFIC RESISTANCE (Ω CM)

10^{12}
10^{11}
10^{10}
10^{9}
10^{8}

ERROR – BARS ARE COMMON TO FIGS. 4.10 – 4.17

3   4   5

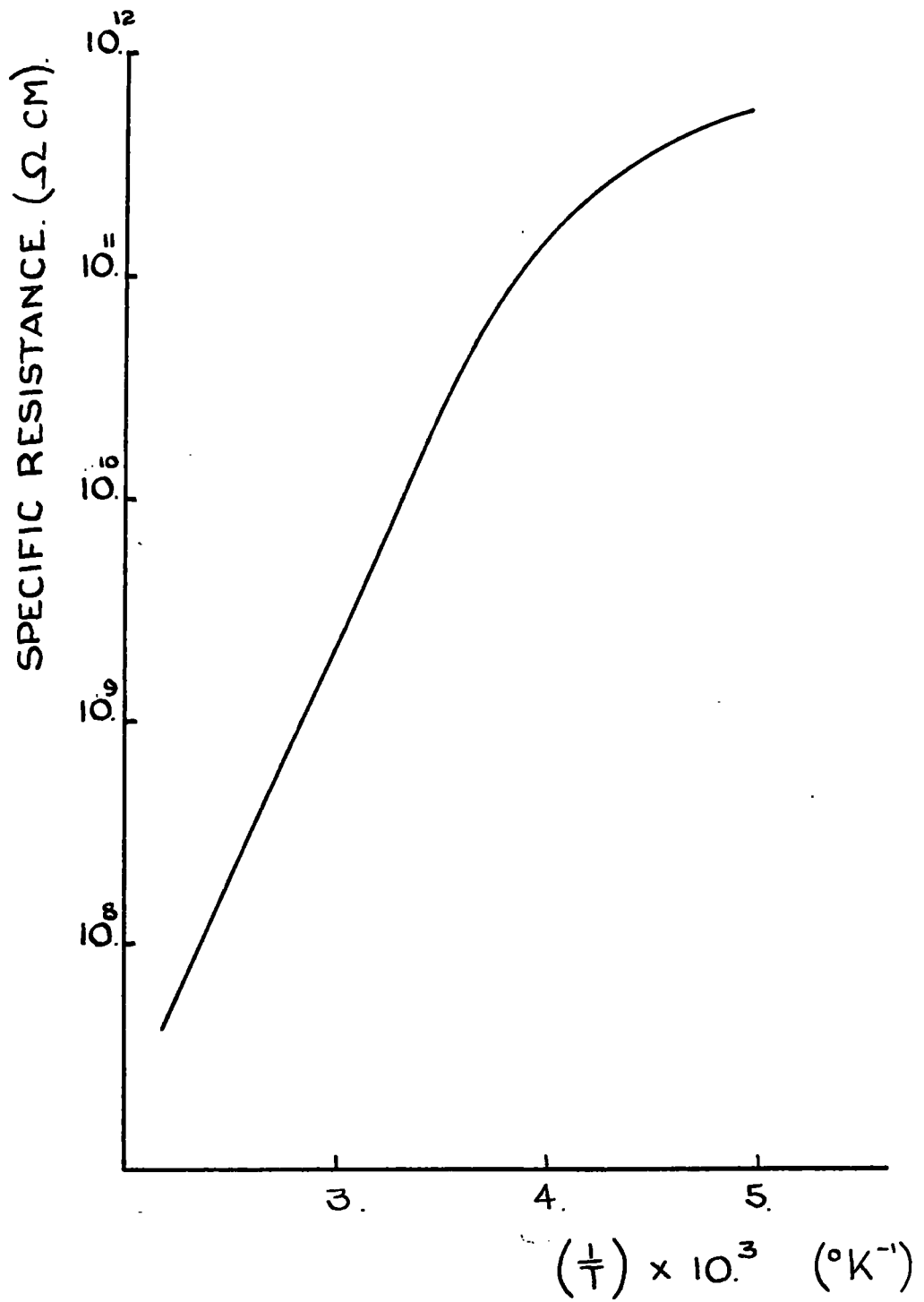$\left(\frac{1}{T}\right) \times 10^3$ ($^\circ K^{-1}$)
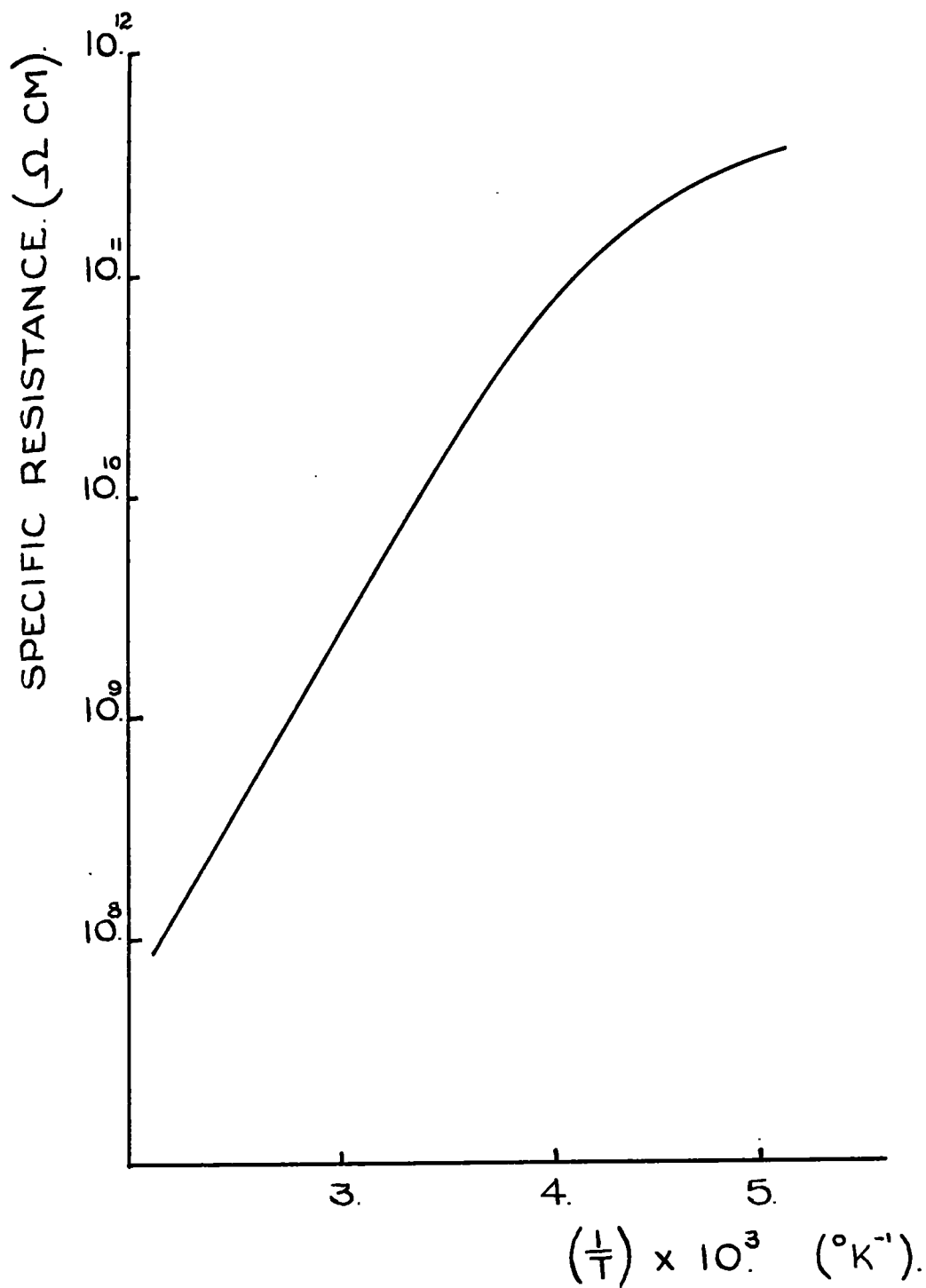
SODA GLASS STANDARD.

FIG. 4.10

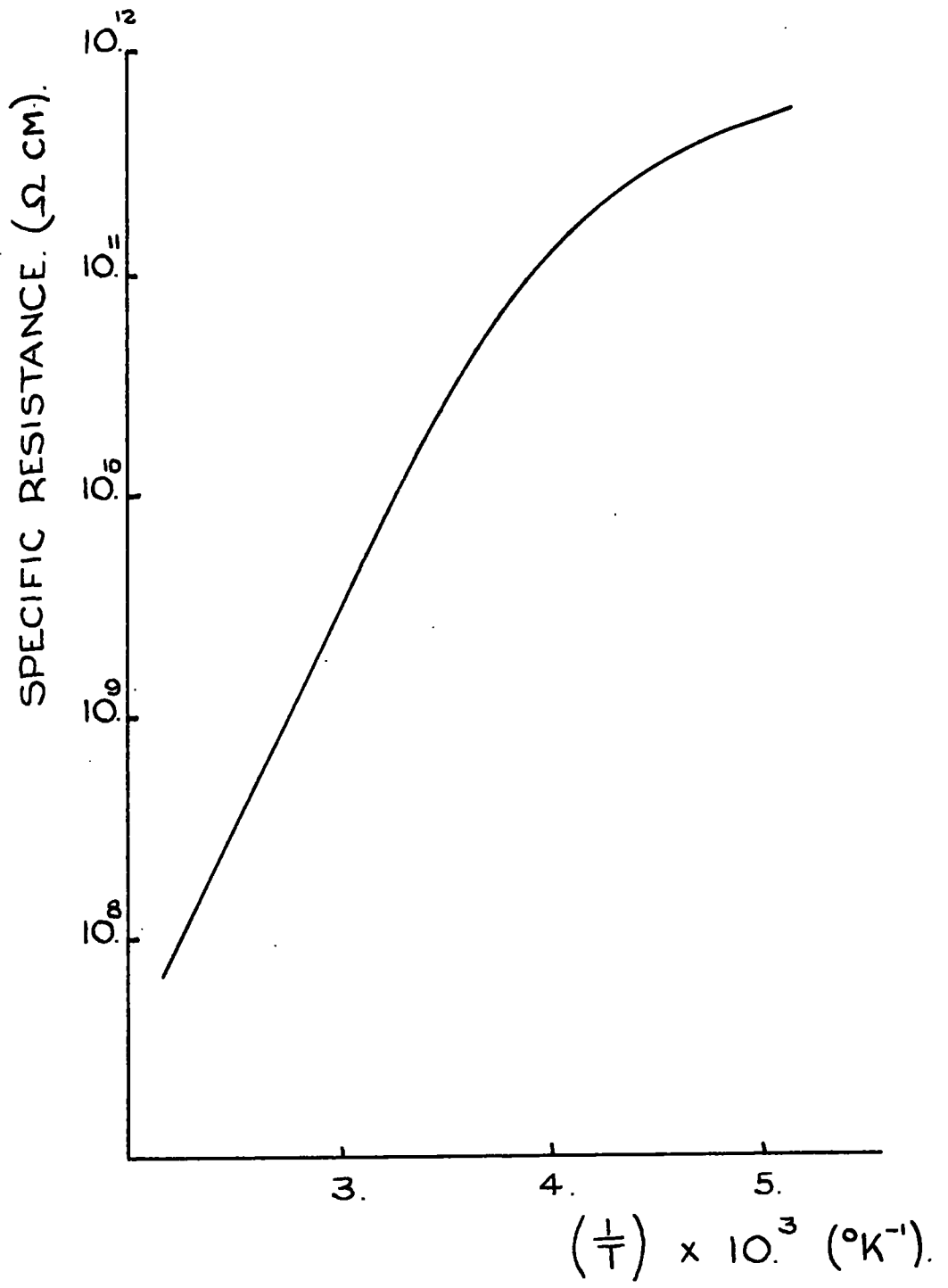5% (BY WT.) PRASEODYMIUM OXIDE IN SODA GLASS.

FIG. 4.11

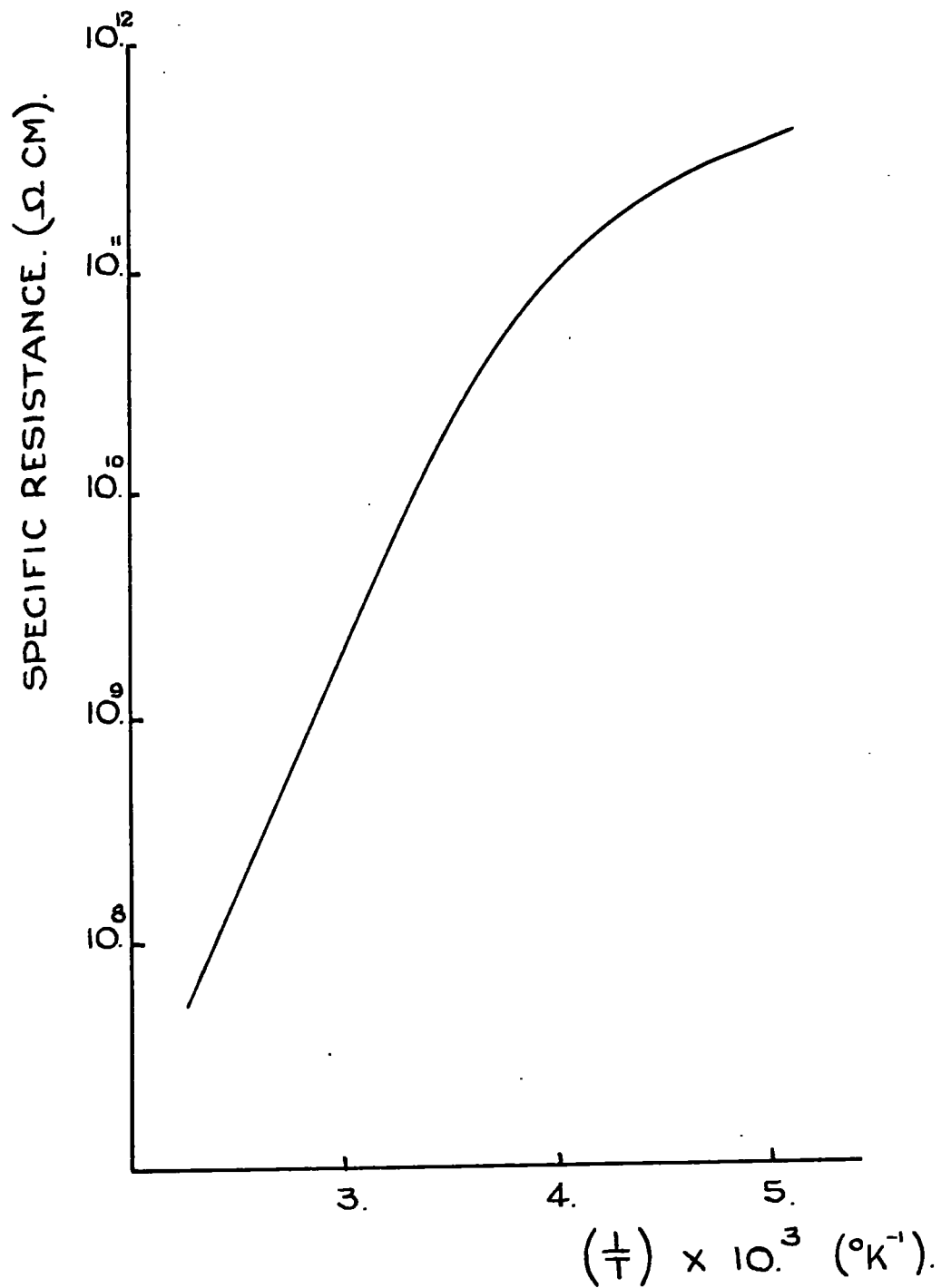5% (BY WT.) NEODYMIUM OXIDE IN SODA GLASS.

FIG. 4.12

5% (BY WT.) SAMARIUM OXIDE IN SODA GLASS.
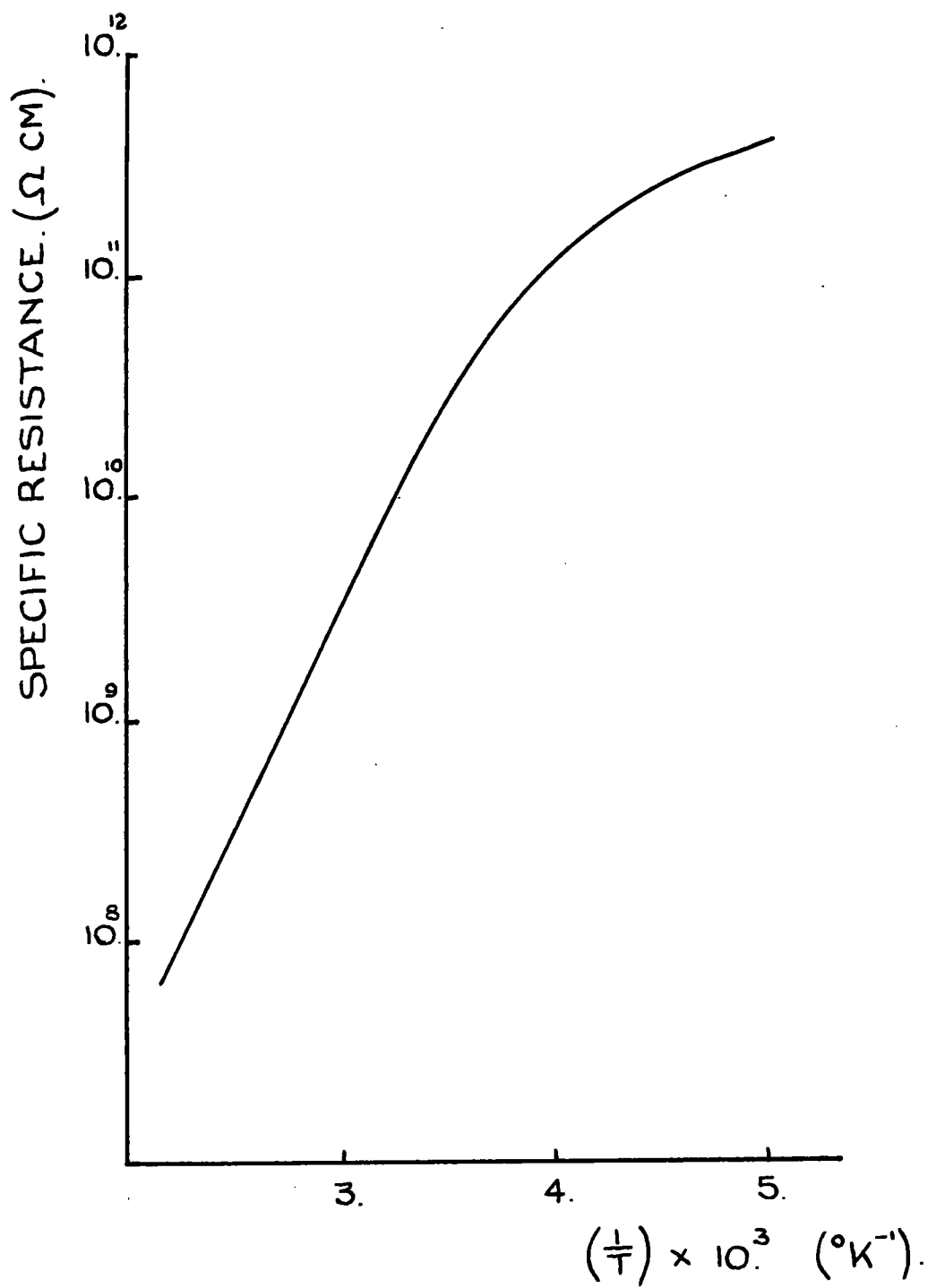
FIG. 4.13

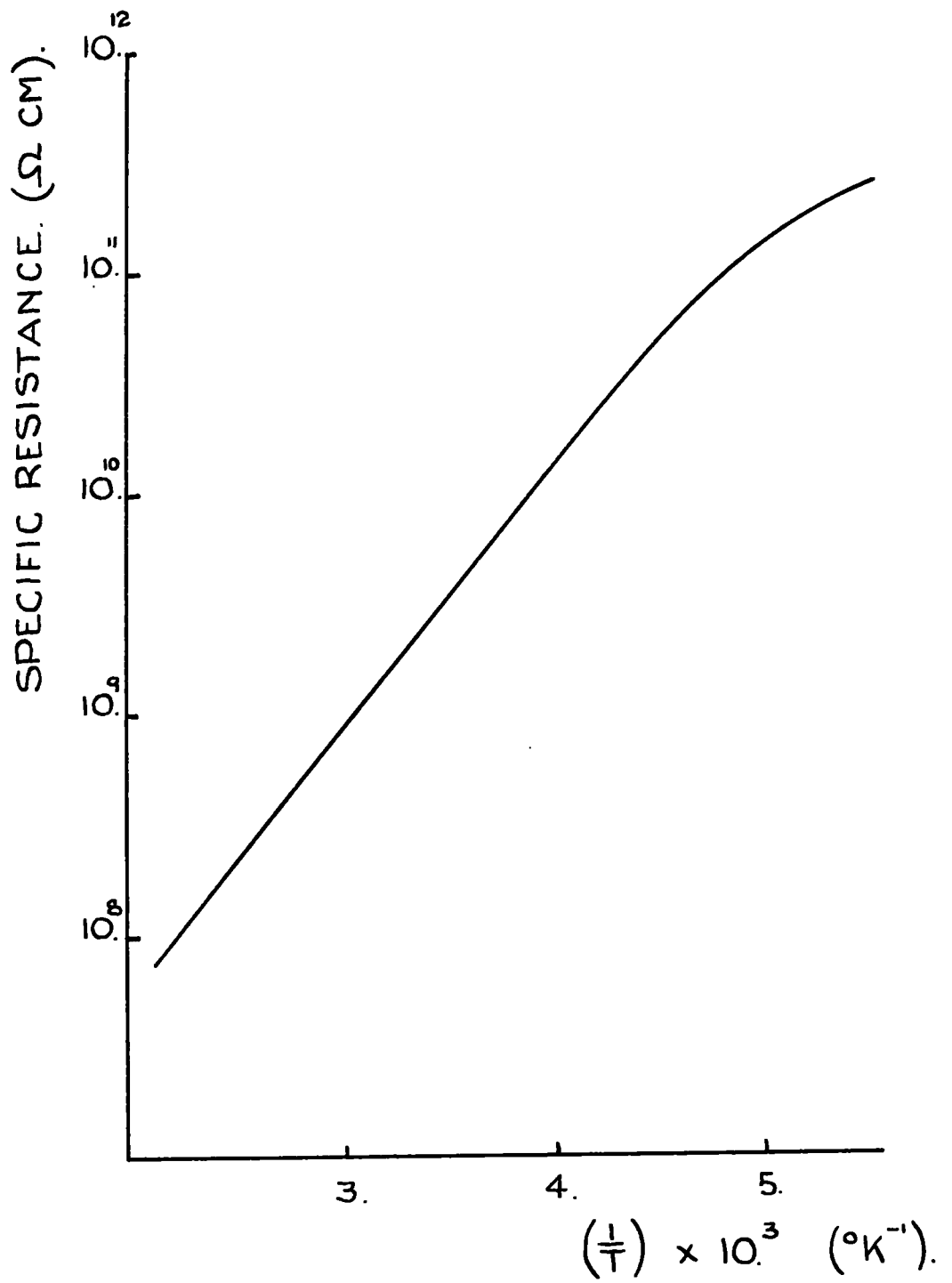5% (BY WT.) GADOLINIUM OXIDE IN SODA GLASS.

FIG. 4.14

10% (BY WT.) GADOLINIUM OXIDE IN SODA GLASS.

FIG. 4.15

5% (BY WT.) DYSPROSIUM OXIDE IN SODA GLASS.

FIG. 4.16

5% (BY WT.) ERBIUM OXIDE IN SODA GLASS.

FIG. 4.17

One would expect a linear relationship to exist between the energy gap and the ionic radius of the specimens examined if the main criterion is one of an included ion impeding the sodium ion migration. Figure 4.18 shows the relationship between activation energy and the rare earth elements tabulated in order of atomic number and Figure 4.19 the relationship between specific resistance at 300°K and the rare earth elements tabulated in order of atomic number. These curves are far from being linear and bear a distinct resemblance to the ionic moment variation across the lathanides shown in Figure 5.8 of the magnetic susceptibility section. Furthermore, increased oxide concentration (ref. gadolinium oxide) does not increase the energy gap but leads to a decrease in A.

One might conclude that the magnetic scattering is partly responsible for the observed variations but it is not clear just how this occurs for ionic current carriers. The anomalous behaviour of the specimen containing erbium oxide is without explanation. It is possible that the erbium ion takes part in the conduction process since it is the smallest of the ions examined and has an ionic radius less than that of Na^{+}. This is not reflected in the conductivity of the specimen containing dysprosium ions which have radii comparable with those of the erbium ions.
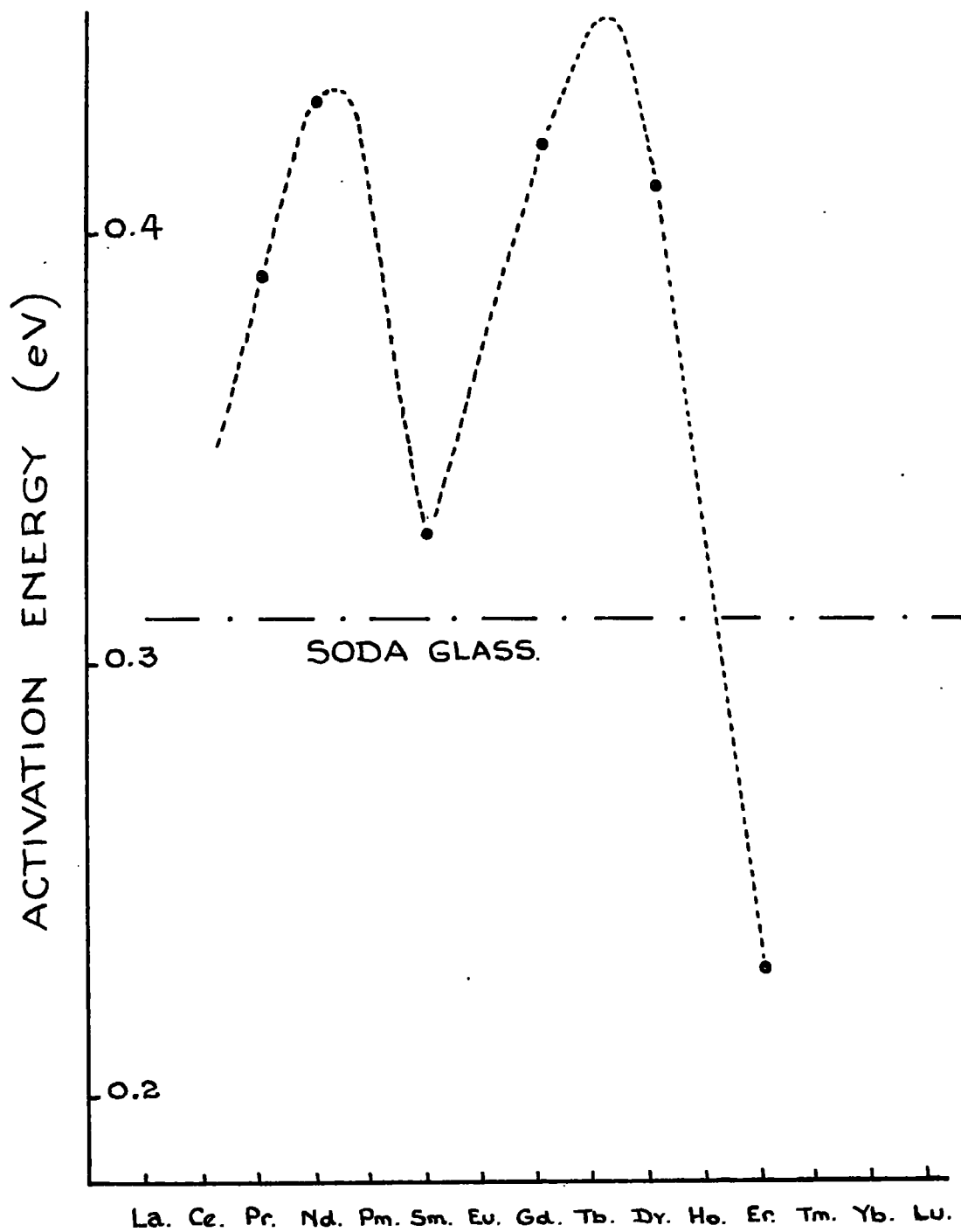
THE RELATION BETWEEN ACTIVATION ENERGY AND THE RARE EARTH ELEMENTS TABULATED IN ORDER OF ATOMIC NUMBER.

FIG. 4.18
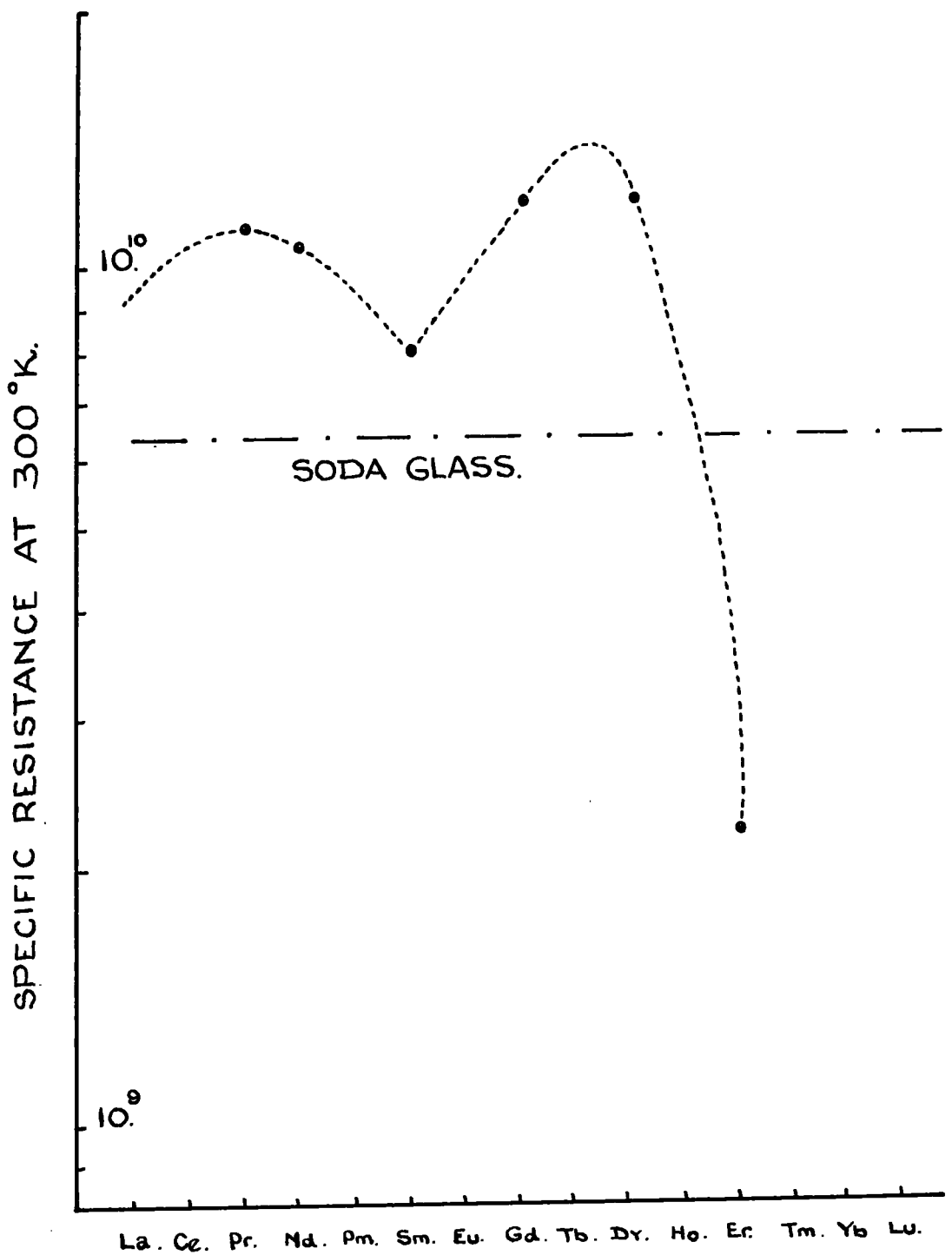
THE RELATION BETWEEN SPECIFIC RESISTANCE
AT 300°K AND THE RARE EARTH ELEMENTS
TABULATED IN ORDER OF ATOMIC NUMBER.

FIG. 4.19
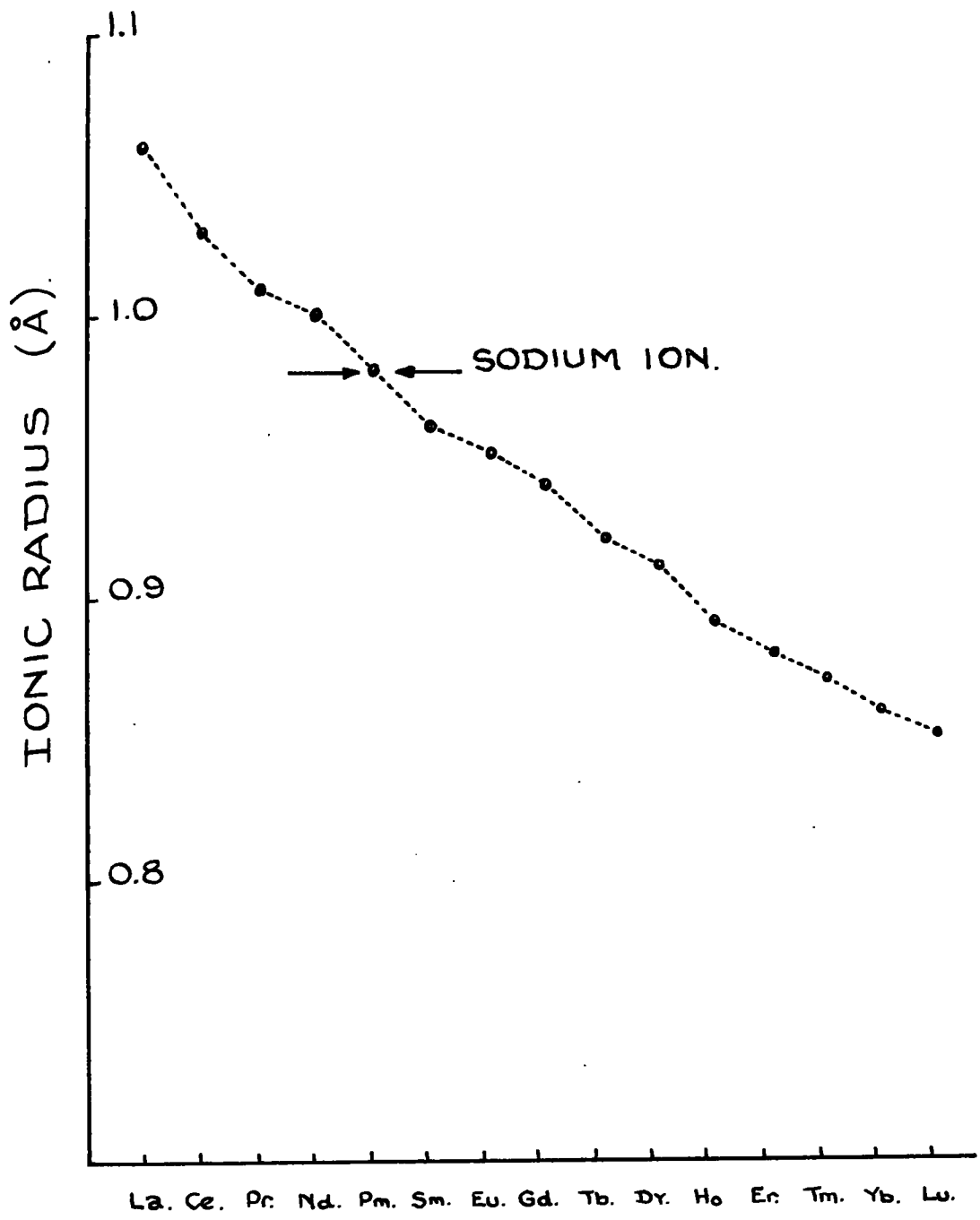
THE IONIC RADII OF THE RARE EARTH ELEMENTS.

FIG. 4.20

As an extension of this investigation one might suggest a comparative study of specimens containing gadolinium oxide and yttrium oxide. This would help to establish whether or not a magnetic factor is involved in the conductivity by eliminating the size factor. Further studies on gadolinium oxide and others at concentrations less than 5% should indicate the growth of a magnetic contribution.

CHAPTER FIVE.

MAGNETIC SUSCEPTIBILITY MEASUREMENTS.

5.1 Introduction.

In 1895 Pierre Curie showed that substances containing permanent magnetic dipoles have a temperature dependent and field independent susceptibility given by

$$\chi = \frac{C}{T}$$

where T is the absolute temperature and C is called the Curie constant. Substances that obey Curie's law, at least to a first approximation, are usually called normal paramagnets.

5.2 A Theoretical Derivation of Curie's Law.

Suppose we have a volume of gas containing N paramagnetic atoms per unit volume, each with a permanent moment μ. There will be no net magnetisation of the gas because the moments are kept in a state of random orientation by the thermal agitation of the gas atoms. If a magnetic field is applied the dipoles will tend to orientate themselves in the direction of the applied field. This will be opposed by the thermal agitation and complete alignment will only be achieved at absolute zero. At any temperature above absolute zero a state of equilibrium is reached between the

aligning and disruptive elements. In the calculation of M,

the net magnetisation per unit volume in the field direction,

it will be assumed that each dipole feels only the applied

field H i.e., no dipole interaction.

In the first instance we will also assume that all the

atoms are in their ground state characterised by J, the

angular momentum quantum number. This implies that, compared

with the thermal energy kT, the J states are widely spaced;

that is $E_{J'}^{j} - E_J \gg kT$. The permanent atomic magnetic

moment can have the components $M_J \cdot g \cdot \mu_B$ in the field

direction, where $M_J = J(J \div 1)$------, $-(J - 1)$, $- J$, and

each dipole a potential energy $- M_J \cdot g \cdot \mu_B \cdot H$. Then, the number

of atoms with a particular orientation will be given by the

Boltzmann factor $e^{M_J \cdot g \cdot \mu_B \cdot H / kT}$. We then get

$$M = N \cdot \frac{\sum\limits_{-J}^{+J} M_J \cdot g \cdot \mu_B \cdot e^{M_J \cdot g \cdot \mu_B \cdot H / kT}}{\sum\limits_{-J}^{+J} e^{M_J \cdot g \cdot \mu_B \cdot H / kT}} \qquad \text{-------(1)}$$

For magnetic fields produced in the laboratory

$M_J \cdot g \cdot \mu_B \cdot H / kT \ll 1$ and the above equation may be written

$$M = N \cdot g \cdot \mu_B \frac{\sum\limits_{-J}^{+J} M_J (1 + M_J \cdot g \cdot \mu_B \cdot H / kT)}{\sum\limits_{-J}^{+J} (1 + M_J \cdot g \cdot \mu_B \cdot H / kT)}$$

Now terms of the type $\sum\limits_{-J}^{+J} = 0$, whereas

$$\sum\limits_{-J}^{+J} 1 = 2J + 1 \quad \text{and} \quad \sum\limits_{-J}^{+J} M_J^2 = \frac{J(J + 1)(2J + 1)}{3}$$

We then get

$$M = \frac{Ng^2 J(J + 1)\mu_B^2 H}{3kT}$$

so that the susceptibility is

$$\chi = \frac{Ng^2 J(J + 1)\mu_B^2}{3kT} \qquad \text{-------(2)}$$

$$= \frac{N\mu^2}{3kT} \qquad \text{-------(3)}$$

$$= \frac{N p_{eff}^2 \mu_B^2}{3kT} \qquad \text{-------(4)}$$

where the effective number of Bohr magnetons is given by

$$p_{eff} = g\left[J(J + 1)\right]^{\frac{1}{2}} \qquad \text{-------(5)}$$

$$= \frac{(3\chi kT)^{\frac{1}{2}}}{N\mu_B} \qquad \text{-------(6)}$$

Curie's law is obtained from equation (3), often referred to as the Hund expression, with $C = N\mu^2/3k$.

If we now consider the case where the spacing is of the same order as kT there will be an additional contribution to the susceptibility due to thermal excitation into the higher levels. The atoms with a certain value of J will still contribute to the susceptibility according to equation (2). The total susceptibility will be obtained by

summing over all the atoms in different states. The number

of atoms with a given J value will be proportional to the

Boltzmann factor and the degree of degeneracy of the level,

that is (2J+1). We then get

$$\chi = N \cdot \frac{\sum\limits_{J=[L-S]}^{L+S} \left\{ \left[g_J^2 \cdot \mu_B^2 \cdot J(J+1)/3kT \right] + \alpha(J) \right\} (2J+1) e^{-\frac{E(J)}{kT}}}{\sum (2J+1) e^{-E(J)/kT}}$$

This additional contribution is called the second order

Zeeman or Van Vleck paramagnetism $\left[\alpha(J) \right]$ and is temperature

independent at low temperatures.

E(J) is the separation $\triangle$ between the levels with

$$N\alpha(J) = \frac{N\mu_B^2}{6(2J+1)} \left[\frac{F(J+1)}{E_{J+1} - E_J} - \frac{F(J)}{E_J - E_{J-1}} \right]$$

where E_{J+1} and E_J represent the energies of the J+1 and

J levels and

$$F(J) = \frac{1}{J} \left[(S+L+1)^2 - J^2 \right] \left[J^2 - (S-L)^2 \right]$$

The existence of this contribution has been observed

experimentally in the case of Eu^{3+} and Sm^{3+}.

In a crystal lattice the electrostatic field of the

ions surrounding a reference rare earth atom can remove the

degeneracy of the (2J+1) fold degeneracy of a given J state

as also can the spin orbit coupling effects. In the case of

rare earth ions this latter interaction is appreciably

greater than the crystal field interaction and this leads

to two important consequences:

(i)   that, unlike the ions of the d-transition

elements, J is a good quantum number;

(ii) that the crystal field interaction may be

treated as a perturbation.

This allows the eigen values and eigen functions, and hence

the magnetic moments associated with a 4f ion in a given

environment to be calculated in a straightforward manner.(15)

The nature of the ground state and of the crystal

field split J level depend upon the magnitude of the various

components of the crystal field and reflects directly the

symmetry of the crystalline lattice.

In a glass, where a given impurity atom may find

itself in one of several environments, the detailed ionic

behaviour of an atom will be peculiar to its particular site.

Consequently, analysis of the susceptibility - temperature

relationship of such glasses may be complicated. It is

perhaps worth mentioning at this point that this multiplicity

of sites, and consequently the multiplicity of crystal field

split levels associated with these sites, will give rise to

a much more complex optical spectrum for a given ion than

one would observe for it in a crystalline environment and

also to a more complicated electron spin resonance spectrum.

These two properties have been examined during this study and will be discussed in a later section.

If the individual rare earth ions are capable of a cooperative magnetic interaction then this will lead to a modification of the Curie law and the susceptibility will be of the form:

$$\chi = \frac{C}{T - \theta}$$

where θ is the paramagnetic Curie point.

Such interactions are possible between rare earth ions only through an indirect exchange, for example, the R.K.K.Y. interaction, (16) super exchange or double exchange. The absence of conduction electrons in a glass prevents the most commonly known indirect exchange mechanism, the R.K.K.Y. interaction, from making any contribution to the magnetic behaviour. Since the energy associated with the other interactions is generally very small one can anticipate that the Curie temperatures, if any, for rare earth containing glasses will also be small.

In this study the temperature dependence of the magnetic susceptibilities of the doped glasses previously described was measured by the normal force method. (17) Briefly, this method involves suspending a specimen from one arm of a microbalance by a quartz fibre and recording the
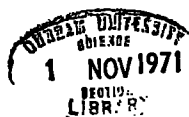
variation in apparent weight for various temperatures when
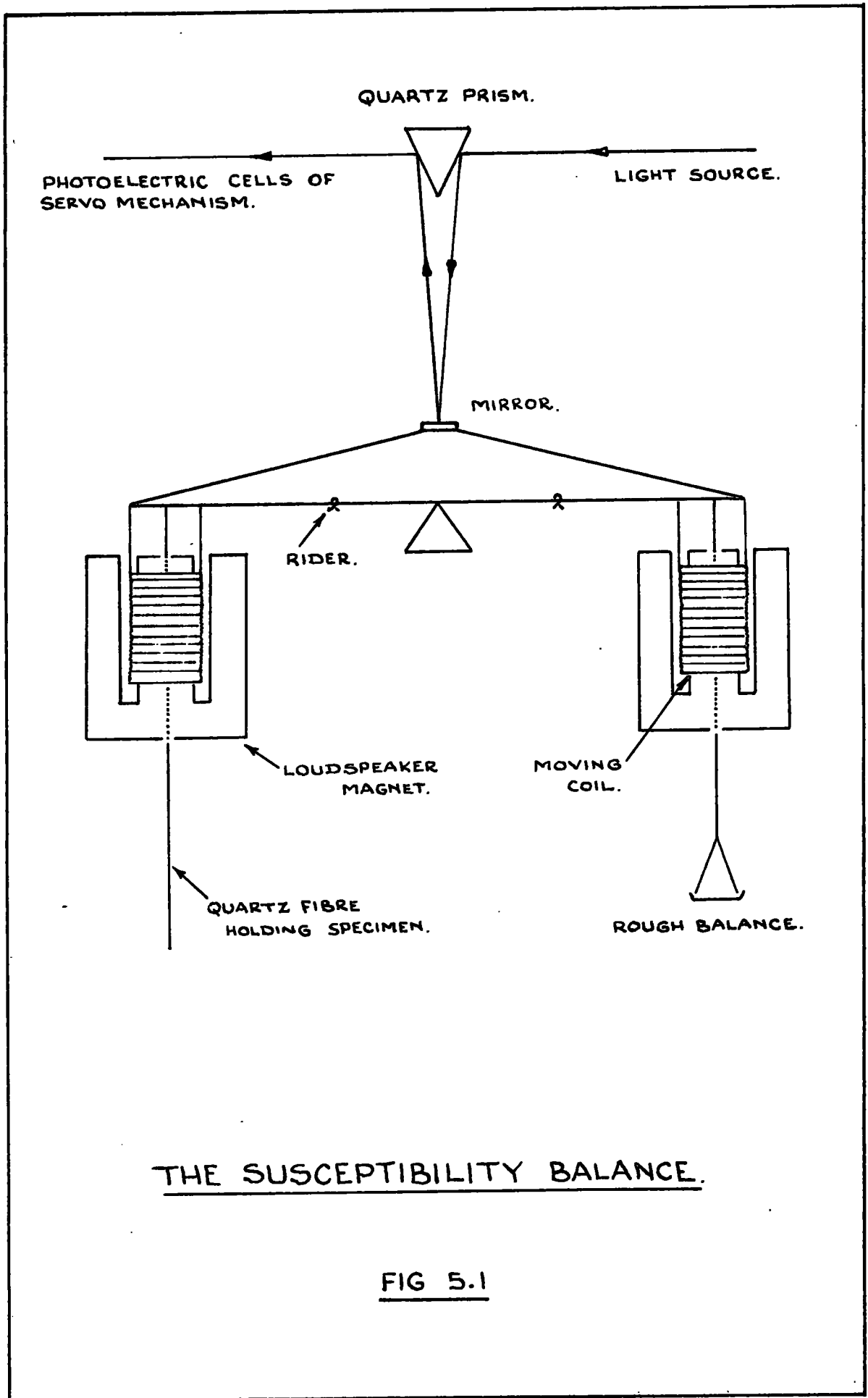the specimen is placed in a field gradient.
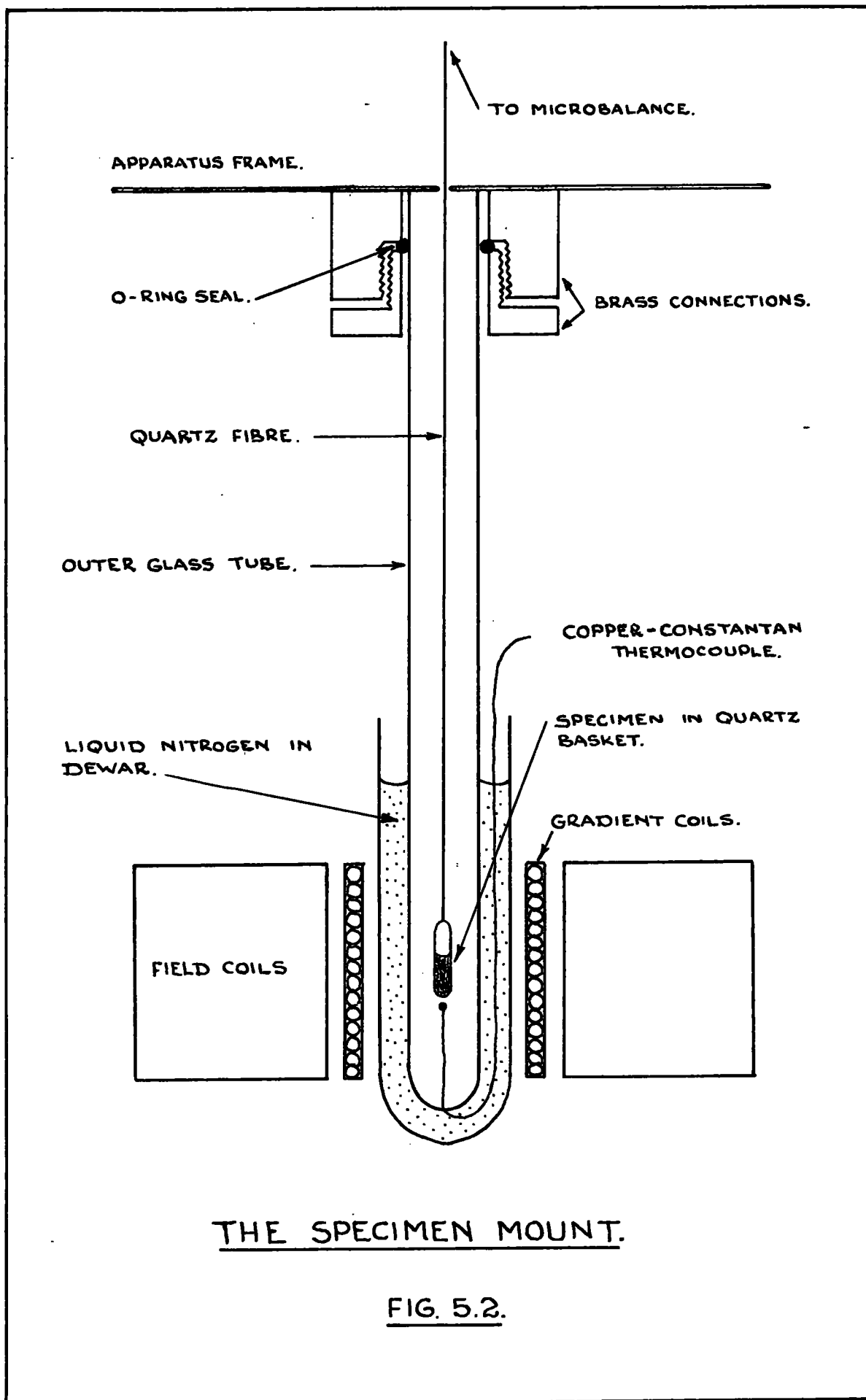
5.3 The Susceptibility Balance.

A diagram of the susceptibility balance is shown in
Figure 5.1. With the specimen and ancillary apparatus in
position the beam riders were adjusted to achieve a balance.
Under such balanced conditions the light reflected down to
the beam mirror by the quartz prism is returned to equally
illuminate two photoelectric cells of a servo-balance
mechanism. This causes equal currents to flow in the loud-
speaker magnet coils situated at each end of the beam and
hence the balance is not disturbed. As the specimen reacts
to the field gradient the beam moves out of its horizontal,
balanced, position thereby altering the cell illumination
and causing unequal currents in the beam magnets. The
circuitry involves a classical servo-amplifier operating
so that the magnitude and direction of the coil current is
continuously adjusted to maintain a balance.

5.4 The Specimen Mount.

A diagram of the specimen mount is shown in Figure 5.2.
The suspended specimen was surrounded by a glass tube
capable of maintaining a vacuum although, during this series
of experiments, it was filled with dry helium gas. As
mentioned previously the presence of the gas not only

QUARTZ PRISM.

PHOTOELECTRIC CELLS OF SERVO MECHANISM.

LIGHT SOURCE.

MIRROR.

RIDER.

LOUDSPEAKER MAGNET.

MOVING COIL.

QUARTZ FIBRE HOLDING SPECIMEN.

ROUGH BALANCE.

THE SUSCEPTIBILITY BALANCE.

FIG 5.1

TO MICROBALANCE.

APPARATUS FRAME.

O-RING SEAL.

BRASS CONNECTIONS.

QUARTZ FIBRE.

OUTER GLASS TUBE.

COPPER-CONSTANTAN THERMOCOUPLE.

SPECIMEN IN QUARTZ BASKET.

LIQUID NITROGEN IN DEWAR.

GRADIENT COILS.

FIELD COILS

THE SPECIMEN MOUNT.

FIG. 5.2.

prevents condensation at low temperatures but also provides a heat transfer medium between the specimen and the surrounding liquid nitrogen. A copper - constantan thermo-couple junction was introduced through the bottom of the tube to a position immediately below the specimen. This junction was again capped by a glass bead.

5.5 <u>The Power Supply.</u>

The power supply for the solenoid was a Brentford stabilised D.C. Power Unit giving a maximum D.C. output of 250V, 300A. Adjustment of this output was done via a remote control unit sited beside the susceptibility balance.

5.6 <u>The Solenoid.</u>

The solenoid consisted of a stack of flat coils of copper strip separated from each other by insulating spacers mounted on a central tube. The coils are electrically connected. A watertight casing allowed forced circulation of deionized cooling water. The field produced was linear with current, giving 42 oersteds per ampere at the centre of the solenoid. Field gradient coils, mounted on a brass tube, were situated in the central tube of the solenoid and supplied, via a rheostat, by the 24 volt D.C. bench supply. The solenoid and field coils were raised and lowered from the operational position by a lifting platform.

5.7 Experimental Method.

The glass tube enclosing the suspended specimen was evacuated and filled with dry helium gas.

As a preliminary to the susceptibility measurements it was necessary to centralise the specimen in the solenoid. This was achieved by raising the solenoid incrementally and recording the balancing current supplied by the servo-mechanism. This current was measured on a Scalamp D.C. microammeter. The lifting platform was then clamped into the position requiring maximum current at room temperature.

The specimen was cooled to $84^{\circ}K$ by a surrounding polystyrene dewar filled with liquid nitrogen. Polystyrene, being porous, made a most satisfactory container in that the nitrogen could slowly leak away after the minimum temperature had been reached thereby allowing only a gradual return to room temperature. The solenoid power unit was set to give a stabilised voltage supply of 95V, 120A. As the specimen gradually warmed to room temperature the magnitude of the balancing current, again measured on a Scalamp D.C. microammeter, was recorded at various temperatures in the range $84^{\circ}K$ to $291^{\circ}K$.

It was found that, of the prepared specimens, only those containing 10% Gd_2O_3, 5% Gd_2O_3, 5% Dr_2O_3 and 5% Er_2O_3 caused measurable balancing currents. The data obtained

using a pure Gd_2O_3 specimen was used to calibrate the apparatus.

5.8 Results.

The data obtained for this series of measurements is shown graphically in Figure 5.3 through to Figure 5.7.

P.W. Selwood in his book "Magnetochemistry" (18) gives the susceptibility of gadolinium oxide, at $293^{\circ}K$, as being 135×10^{-6} emu.g^{-1} . Using this figure in conjunction with the observed results for gadolinium oxide, shown graphically in Figure 5.3, it was possible to evaluate a calibration constant for the apparatus as follows:

$$\Delta I = k.H_z. \frac{dH_z}{dz} .m. \chi$$

where ΔI represents the restoring current,

H_z the applied field,

$\frac{dH_z}{dz}$ the field gradient,

m   the mass of the specimen,

χ the susceptibility,

and k is a proportionality constant.

Also, under the experimental conditions imposed

$$k. H_z. \frac{dH_z}{dz} . = k' \text{ (the calibration constant)}$$

Thus $\Delta I = k'.m. \chi$ from which k' may be evaluated given that $\chi_{(293)} = 135 \times 10^{-6}$ emu.g^{-1} , $\Delta I = 335.6$mm and m $= 67 \times 10^{-3}$ g.

$$k' = 37 \times 10^{6} \text{ mm.emu}^{-1} .$$

The Curie - Weiss constant and the effective Bohr magneton number for each of the specimens examined can now be calculated.

For example, in the case of the gadolinium oxide (5%) containing specimen

$$(1/\chi_{200}) = (1/\Delta I_{200}) \cdot k' \cdot m$$

$$= 87.95 \times 10^3 \text{ g.emu}^{-1}.$$

and
$$(1/\chi_{100}) = 38.80 \times 10^3 \text{ g.emu}^{-1}.$$

Curie constant (C) $= \dfrac{\Delta T}{(1/\chi)} = 2.04 \times 10^{-3} \text{ K.emu.g}^{-1}.$

As shown by equation 6 in the introduction to this section

$$\rho_{eff} = \left(\frac{3k}{N\mu_B}\right)^{\frac{1}{2}} \cdot \left(\frac{\Delta T}{(1/\chi)}\right)^{\frac{1}{2}}$$

$$= 2.84 \left(2.04 \times 10^{-3} \times 20 \times \frac{362}{2} \right)^{\frac{1}{2}}$$

the Curie constant now being in terms of 1 mole of gadolinium oxide as opposed to 1 gramme of glass.

Thus $\rho_{eff} = 7.7\mu_B.$

By this method the Curie - Weiss constant and the effective Bohr magneton number were calculated for each of the specimens examined. These parameters are tabulated along with the paramagnetic Curie points in Table 5.1.
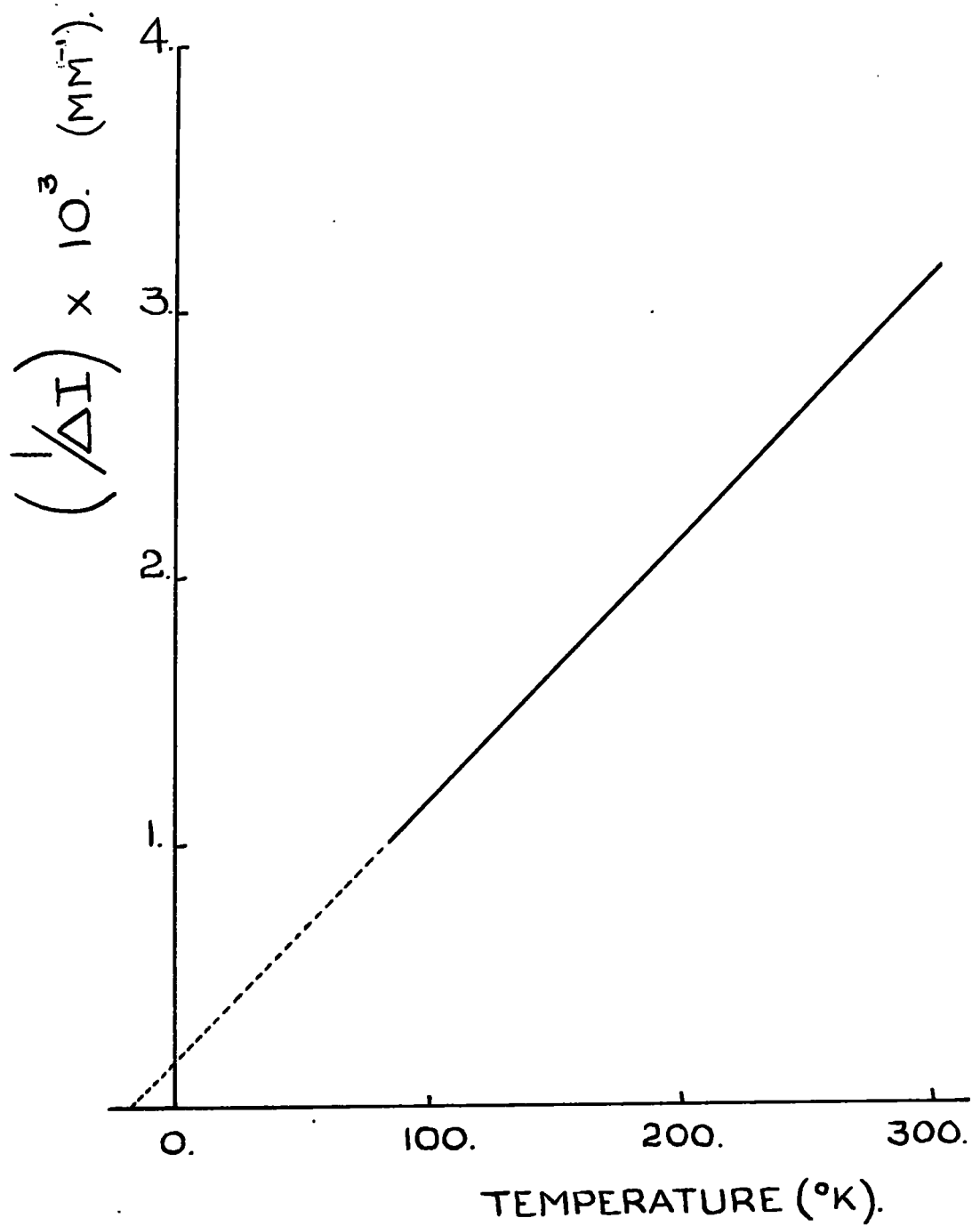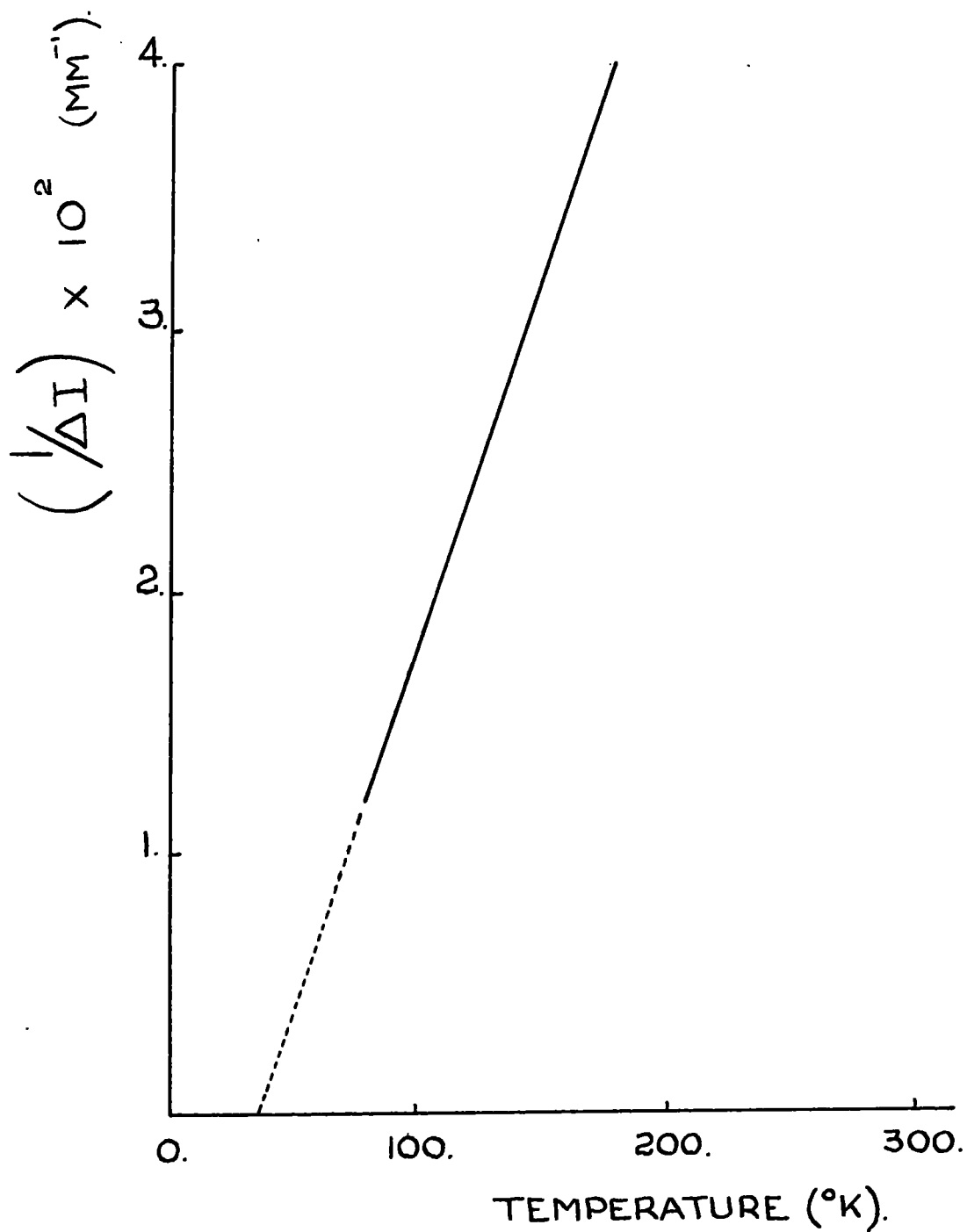
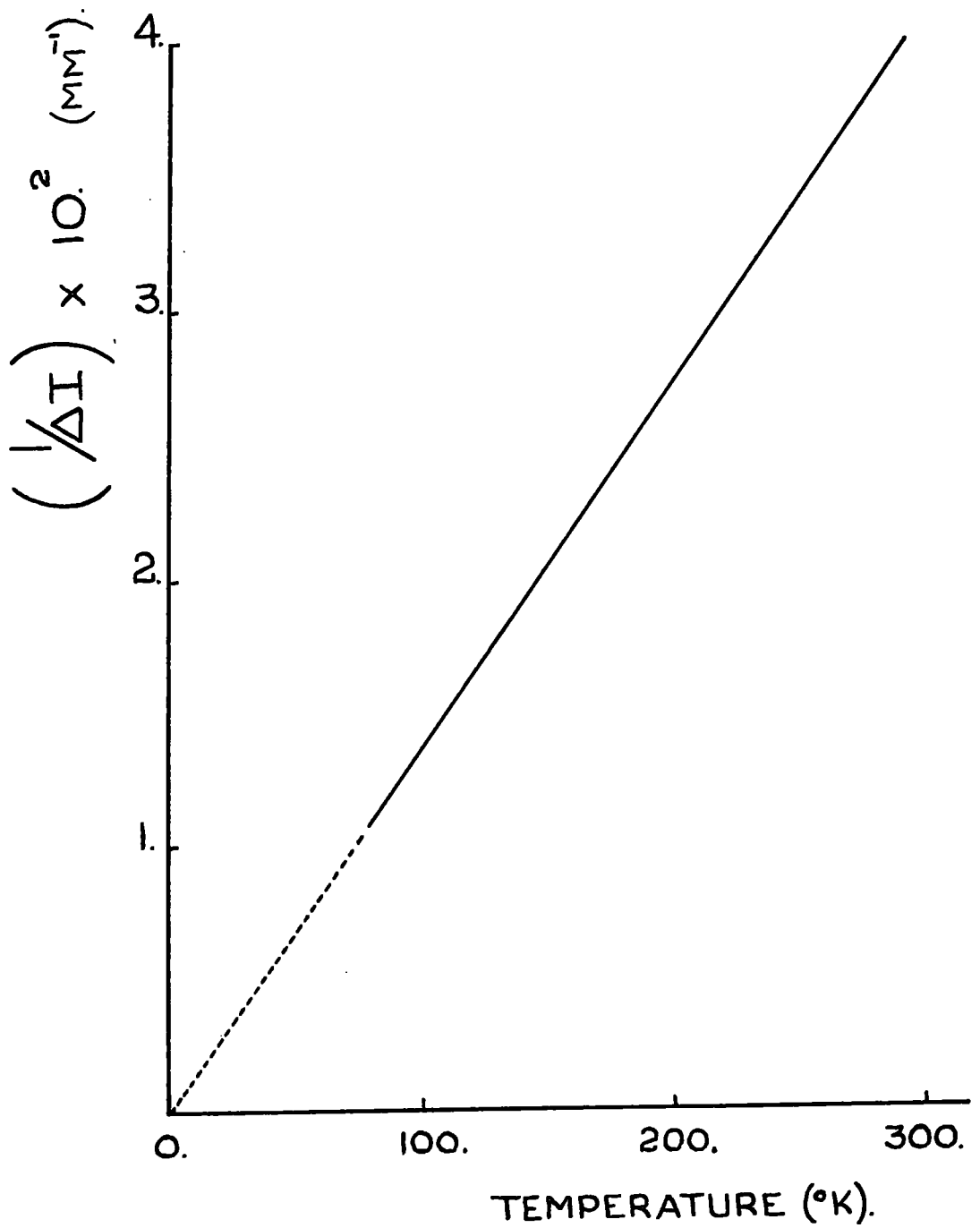GADOLINIUM OXIDE CALIBRATION CURVE.

FIG. 5.3
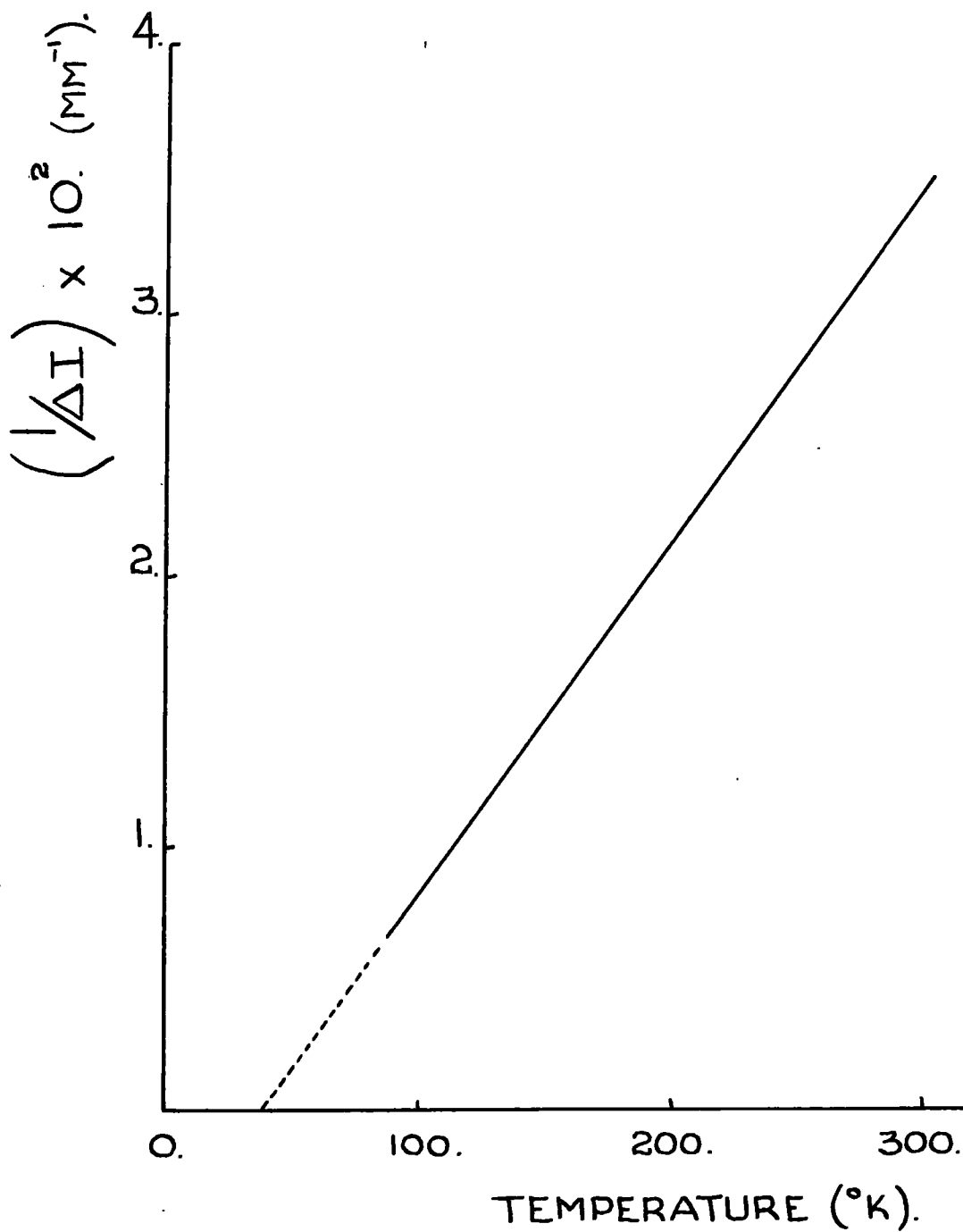
10% (BY WT.) GADOLINIUM OXIDE IN SODA GLASS.
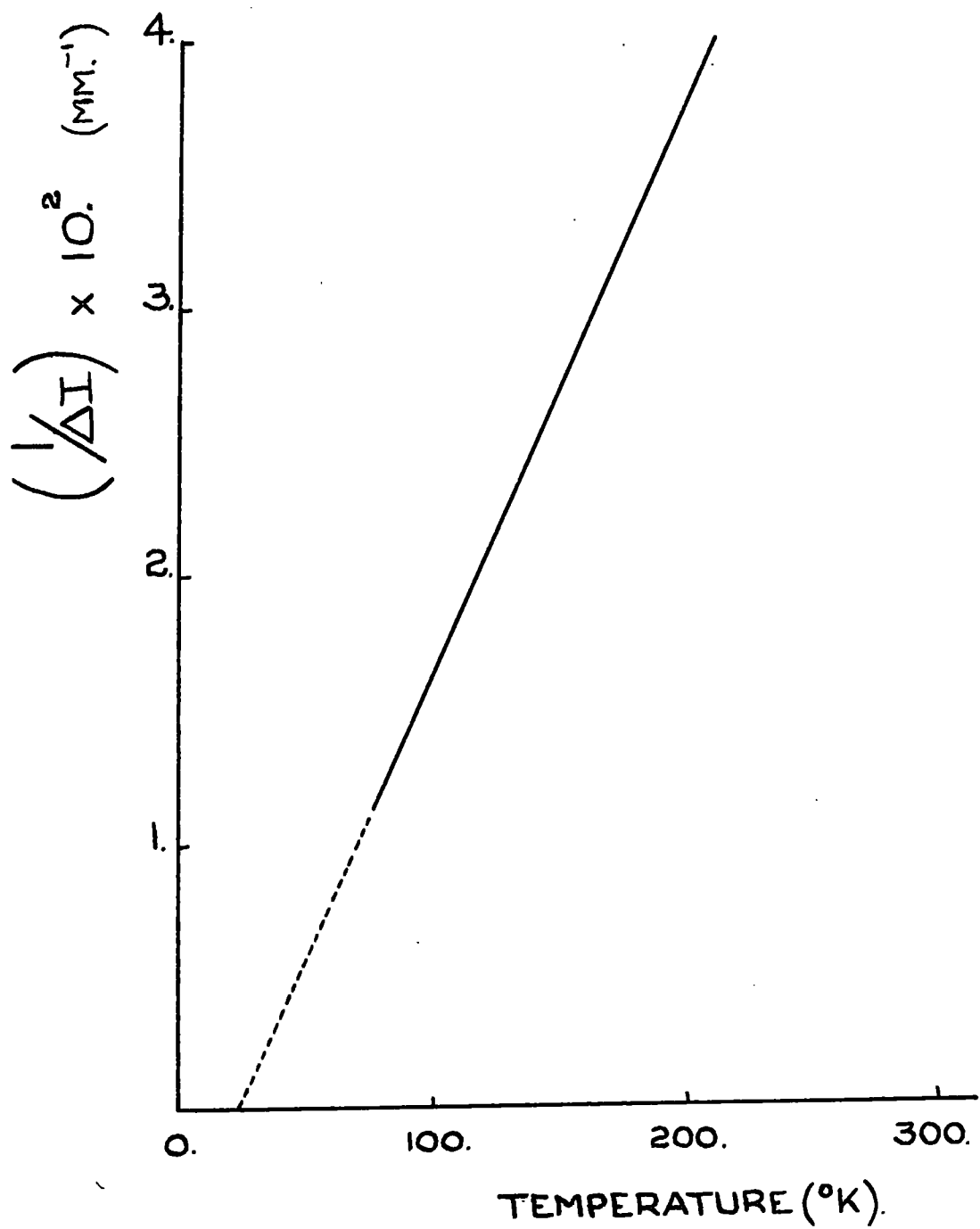
FIG. 5.4

5% (BY WT.) GADOLINIUM OXIDE IN SODA GLASS.

FIG. 5.5

5% (BY WT.) DYSPROSIUM OXIDE IN SODA GLASS.

FIG. 5.6

5% (BY WT.) ERBIUM OXIDE IN SODA GLASS.

FIG. 5.7

SPECIMEN. (SODA GLASS PLUS)	THIS RESEARCH.			LITERATURE ON PURE OXIDES.			$p_{eff.}$ (VAN VLECK) FIG. 5.8
	$C.$ (K.emu.At^{-1})	$\theta.$ (°K).	$p_{eff.}$ (μ_B).	$C.$ (K.emu.At^{-1})	$\theta.$ (°K).	$p_{eff.}$ (μ_B).	
5% (BY WT.) Gd_2O_3.	7.4	35.	7.7	7.7	−18.	7.8	7.94
10% (BY WT.) Gd_2O_3.	7.4	37.	7.7	7.7	−18.	7.8	7.94
5% (BY WT.) Dy_2O_3.	14.7	2.	10.9	13.9	−21.	10.4	10.60
5% (BY WT.) Er_2O_3.	9.6	23.	8.8	11.1	−13.	9.4	9.58

TABLE 5.1
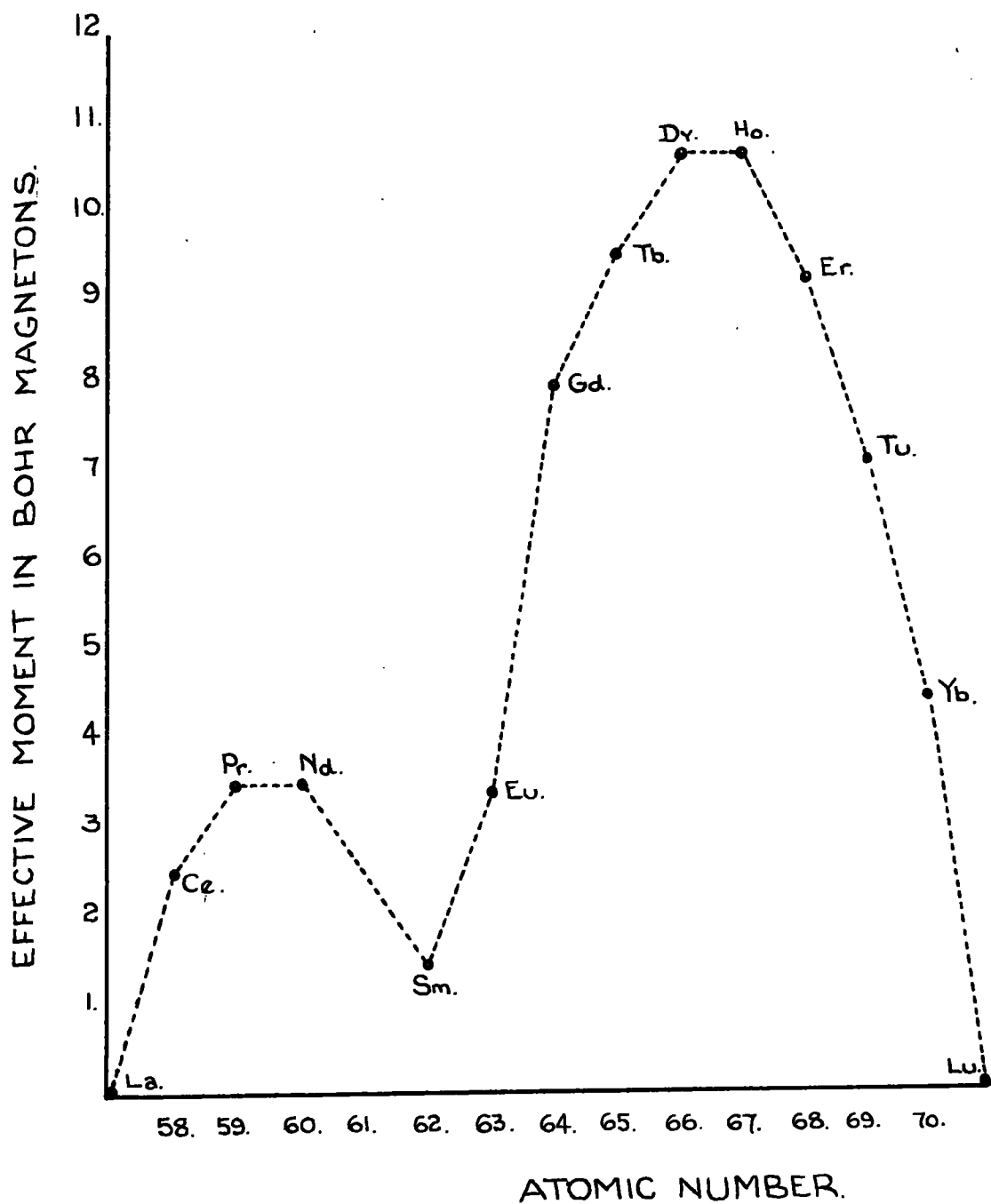
EFFECTIVE BOHR MAGNETON NUMBERS FOR
THE TRIVALENT IONS OF THE RARE EARTHS
AT ROOM TEMPERATURE.

FIG. 5.8

The specimens containing gadolinium ions lead to an effective Bohr magneton number which is in good agreement with values quoted (19) for pure gadolinium oxide but lies somewhat below the theoretical number calculated from the appropriate equations of Van Vleck on the basis of free ions.

The results obtained for the dysprosium oxide doped specimen show that the Bohr magneton number associated with the dysprosium ion is of the same order of magnitude as the ionic number. It is however, significantly greater than values quoted for pure dysprosium oxide.

The number associated with the erbium ion in the erbium oxide doped specimen would indicate that a considerable amount of quenching has taken place as a result of the 'crystalline' electric field in the glass structure.

It will be shown later that optical properties indicate a significantly greater contribution to the optical absorption line widths, arising from a variation in 'crystalline' electric field within the specimen, in the case of specimens doped with erbium oxide and gadolinium oxide than the dysprosium oxide doped specimen. It is assumed, at this point, that the effect of the 'crystalline' electric field on susceptibility is less for the dysprosium ions than for the others.

Since the gadolinium ion is in an S state, and

therefore spherically symmetrical, it will be relatively insensitive to even the most intense crystalline fields and hence the observed paramagnetic behaviour is comparable with that of the oxide. The included gadolinium ion will, therefore, give little information about the electronic and structural properties of the glass.

The erbium ion, however, is in a $^4I_{\frac{15}{2}}$ state and will be considerably influenced by crystalline field splitting of the J states and one can expect changes in the magnitude of the ground state moments of at least that shown in Table 5.1.

Using the data obtained in optical experiments it is theoretically possible to evaluate this susceptibility provided one is able to find a means of representing the glass matrix in a way which is suitable for crystalline field calculations.

Time has made this approach impossible during the course of this research but work is continuing along these lines.

CHAPTER SIX.

OPTICAL ABSORPTION SPECTRA.

6.1 Introduction.

To reiterate, one may regard a non-crystalline solid as one in which there is a short range order without the long range order of crystals. Thus, the short range environment of each rare earth ion in the soda glass will approximate to a crystalline environment, but the environment is different for each ion. This heterogeneity of ionic environment can usually be described as a distribution of differing environments about an "average" environment. Furthermore, the results obtained in this section would indicate that this "average" environment is that of the oxide single crystal. The absorption spectra to be expected, therefore, must basically be that of the rare earth oxide single crystal modified by the heterogeneity of environment. This modification arises from slight variations in the magnitudes of the crystal-field parameters. The energy-level shifts for ions in different environments will lead to changes in the transition wavelength from ion to ion. This situation produces a broadening of the single spectral line found in the oxide crystal.

With the exception of Nd_2O_3, a review of the literature revealed little information regarding the absorption spectra of the rare earth oxides. Consequently, since the preparation and examination of single crystals is beyond the scope of this research, the neodymium oxide doped glass was the only one of those prepared to be examined in this section.

6.2 Experimental Method.

The absorption spectrum of a neodymium oxide doped specimen, polished to transparency, was obtained using an Optica Recording Grating Spectrophotometer.

6.3 Results.

Figures 6.1a, 6.1b, and 6.1c show graphically the transmittance of the specimen as a function of the wavelength of incident radiation. Using the same horizontal scale the line spectrum of single crystal Nd_2O_3 (20) has been plotted for comparison. Despite the reasonably low (2 $\overset{o}{A}$) resolution of the instrument used, it is possible to correlate the two spectra.
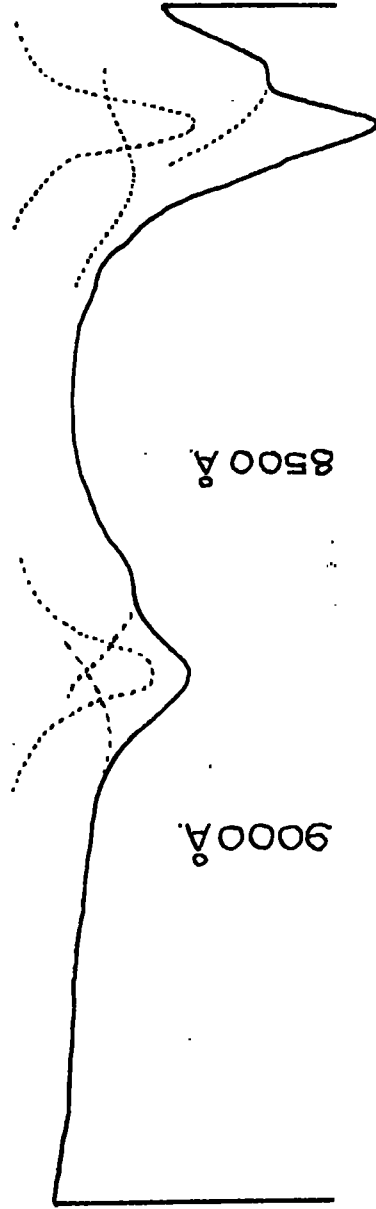
As predicted, the several field splittings, characteristic of an inhomogeneous environment, give rise to spectral broadening and each family of lines in the single crystal spectrum appears as a band. There also appears to be a shift in absorption towards a lower wavelength.

There is a great similarity between the optical

properties of neodymium oxide doped glass and the pure oxide
crystal. This would indicate that the Nd^{3+} ion locates in
only one average environment site in glass mirroring the
fact that there is only one kind of Nd^{3+} ion site in
neodymium sesquioxide having a point group symmetry of C_{3v}.
It is perhaps not unreasonable to conclude from these
observations that any rare earth ion locates in an environment
in glass much like the environment it has in its crystal
form.

NEODYMIUM OXIDE (5%) IN SODA GLASS.

NEODYMIUM OXIDE SINGLE CRYSTAL.

TRANSMITTANCE.

9000 Å

8500 Å

$^4F_{3/2}$

$^4F_{5/2}$

$^2H_{9/2}$

FIG. 6.1 a.

6000 Å

6500 Å

7000 Å

$^4G_{5/2}$

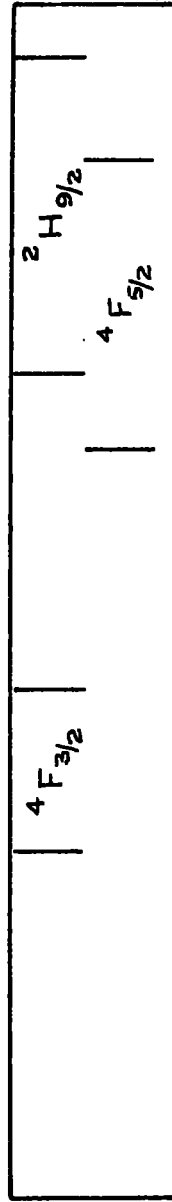$^2G_{7/2}$

$^2H_{11/2}$
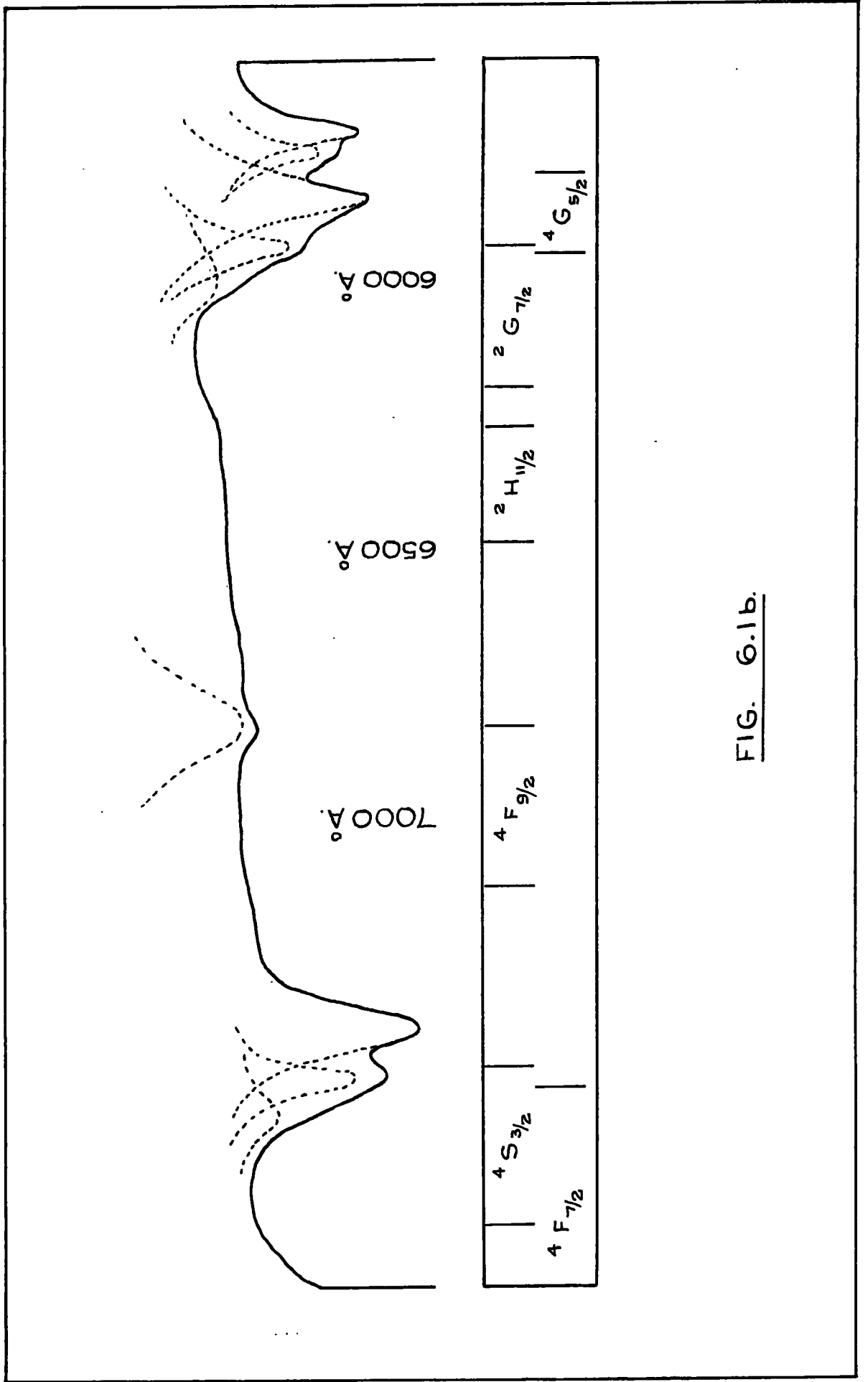
$^4F_{9/2}$

$^4S_{3/2}$
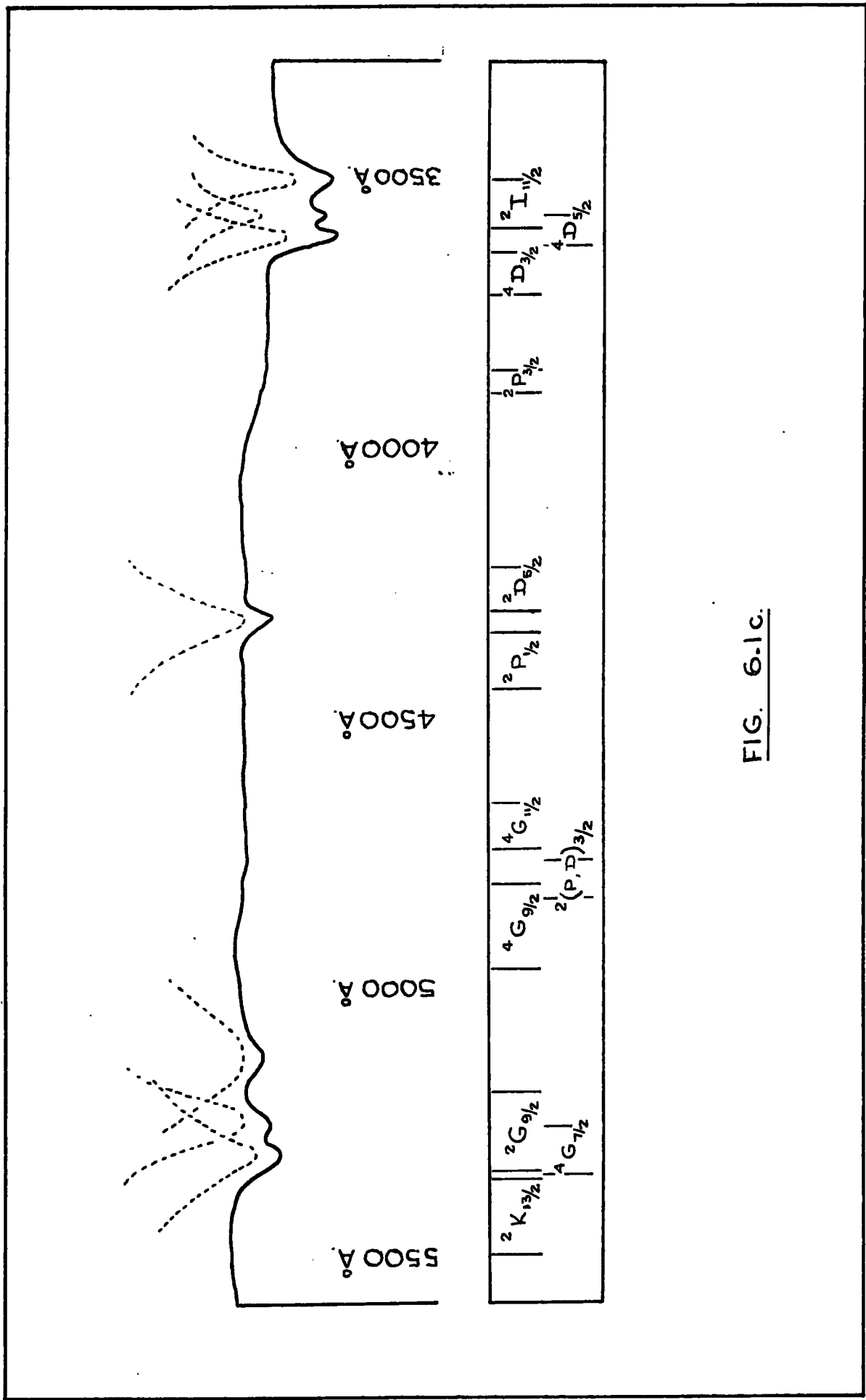
$^4F_{7/2}$

FIG. 6.1b.

FIG. 6.1c.

CHAPTER SEVEN.

ELECTRON SPIN RESONANCE.

7.1 Introduction.

It was pointed out in the introduction to this thesis

that, in the past, most glass studies were concerned with

bulk properties such as viscosity, density, thermal

conductivity etc. Physical techniques that reveal something

of the electronic structure have only become common in

recent years. Some of these techniques have been discussed

in previous sections.

One of the most powerful of the newer physical methods

is electron spin resonance. The primary requirement is that

the substance to be investigated must contain unpaired

electron spins. For the present investigation a simple soda

glass doped with gadolinium oxide has been selected for study.

Details of the specimens prepared are given on page 53.

The rare earths comprise atomic numbers 57 - 71 and,

as we have seen, contain from 1 to 14 electrons in the 4f

shell. We also know that all the ions of this group, except

the end members lanthanum and lutetium, are paramagnetic and

any of these can be introduced into a glass as a probe for

E.S.R. studies. Eu^{2+} and Gd^{3+} have zero orbital angular

momentum and are consequently very attractive for E.S.R. studies. Since the 4f electrons are highly localized they cannot interact with their surroundings via the usual spin-orbit interaction and thus the resonance lines resulting from these ions are relatively narrow and sufficiently intense to be seen at room temperature. The rest of the rare earth ions have wider lines and it is necessary to reduce the temperature to at least $4^{\circ}K$ to observe them.

Many E.S.R. studies have been done on radiation damage in glass, (21) but relatively little has been done by way of substituting magnetic impurity ions in a glass and studying their resonances.

The first E.S.R. study of transition metal ions in glasses was done by Sands (22) who studied some 34 soda-lime-silica glasses. Almost all of his samples had resonances, which he could not explain, at g = 6.0 and g = 4.2. Castner et al (23) assumed crystal field effects to be dominant in their study of iron in soda glass and used a spin Hamiltonian analysis to obtain an isotropic g value of 4.28. This suggested that the resonances observed by Sands were due to impurity Fe^{3+} ions.

Chapeleva et al (24) put gadolinium into a $Tl_2SeAs_2Se_3$ chalcogenide glass and found prominent spectral features at g = 2.0, g = 2.7 and g = 5.9 but offered no theoretical

explanation other than that each resonance was caused by

a strong crystal field in three different sites. Griscom

et al (25) studied Mn^{2+} in both glasses and crystalline

compounds of the lithium borate system and concluded that

the manganese sites in the glasses were probably randomly

distorted versions of the site in the $Li_2OB_2O_3$ compound.

The purpose of the present study is to investigate

the E.S.R. spectra of the Gd^{3+} ion in the soda-silica glass

system at room temperature. The spectra are interpreted with

the aid of a spin Hamiltonian, given by Nicklin, (26) in

the form:

$$\mathcal{H}_s = \mu_B . H . g . S . + D(S_z^2 - \tfrac{1}{3}S(S + 1)) + E(S_x^2 - S_y^2)$$

The analytical results are given in a form which allows

them to be used in interpreting $S = {}^7/2$ spectra such as

those described in this section.

7.2 The Resonance Condition.

Many substances such as organic free radicals, impurity

doped semiconductors, radiation damaged solids and diamagnetic

solids containing small amounts of transition series ions

contain impaired electrons and are thus suited to the E.S.R.

technique. In particular, most of the theory of paramagnetic

resonance in solids was developed from studies of iron and

rare earth group ions which were substituted for 0.1% to

1.0% of the metal ions in diamagnetic salts. This low

concentration of paramagnetic ions allows them to be treated as non-interacting (with each other) and hence they become probes with which to study the local electric fields produced by the non-magnetic surroundings.

The energy of a magnetic moment μ in a magnetic field H is

$$E = -\mu \cdot H$$

We also have that the magnetic moment of an ion is proportional to its total angular momentum so that $\mu \propto \hbar \cdot J$.

or

$$\mu = -g \cdot \mu_B J \qquad = -\gamma \cdot \hbar \cdot J$$
$$= g\left(\frac{-e\hbar}{2mc}\right)J$$

where μ_B is the Bohr magneton.

Thus the Zeeman Hamiltonian for a free ion can be written as

$$\mathcal{H}_z = g \cdot \mu_B \cdot H \cdot J$$

If, for example, we let $H = H_z k$ and use the angular momentum functions $|J, m\rangle$, then

$$\mathcal{H}_z |J, m\rangle = g \cdot \mu_B \cdot H_z J_z |J, m\rangle$$
$$= g \cdot \mu_B \cdot H_z m |J, m\rangle$$

and

$$E_m = \langle J, m| \mathcal{H}_z |J, m\rangle = g \cdot \mu_B \cdot H_z m.$$

are the elctronic Zeeman energy levels for the free ion.

Now suppose for simplicity that $J = \frac{1}{2}$, we then have two energy levels $E_{\pm\frac{1}{2}}$ with the energy separation

$$\Delta E = E_{\frac{1}{2}} - E_{-\frac{1}{2}} = g \cdot \mu_B \cdot H_z$$

the ion can be caused to undergo a transition from the state

$E_{-\frac{1}{2}}$ to the state $E_{+\frac{1}{2}}$ by exposing it to electromagnetic

radiation of frequency ν. Then we have

$$h\nu = \Delta E = g \cdot \mu_B H_z$$

This is the basic resonance relation and shows that the

field and frequency are proportional. It is customary to

define

$$h\nu = g_{eff} \mu_B \cdot H_z$$

where g_{eff} is the effective g value and can be used to

describe any resonance, whether or not the magnetic ion is

a free ion or is incorporated into a solid. In the free ion

case $g_{eff} = g_L$, the Landé g, but in a solid, g_{eff} has

no simple origin because of the complex interactions between

the paramagnetic ion and its surroundings.

Electron spin resonance is useful for studying the

lowest energy levels of an ion, and it turns out that the

splittings of these levels correspond to frequencies in the

microwave region (10^9 to 10^{11} Hz) so that on the frequency

scale the region is above nuclear magnetic resonance and below

infra-red spectroscopy. In principle, the experiment could

be performed by either varying the frequency of the radiation

while holding the field at a fixed value, or by holding the

frequency fixed while sweeping the field. The latter method

is almost always used because most microwave oscillators are

essentially fixed frquency devices.

The resonance signal contains components in-phase and out-of-phase with the incident radiation so that a complex susceptibility can usefully be defined such that

$$\chi = \chi' - i\chi''$$

The dispersion component χ' is in-phase and the absorption χ'' is out-of-phase. The experimental apparatus can be adjusted to detect either component although in this study only the absorption component was obtained.

7.3 The Specimens.

In the present study four specimens were selected for examination. They were:

(i)   soda glass;

(ii)   soda glass doped with 5% (by weight) gadolinium oxide;

(iii) soda glass doped with 10% (by weight) gadolinium oxide;

(iv)   pure gadolinium oxide.

An X-ray powder pattern showed that devitrification had not occurred during the preparation of the doped glass specimens.

7.4 Experimental Method.

A set of resonance spectra were taken with an X band (9.8 GHz) microwave reflection spectrometer at room temperature.

7.5 Results.

The absorption spectra obtained are shown in Figures 7.1 to 7.3, each being the average of six traces. In the case of the undoped soda glass there is zero absorption but for the remainder an appreciable absorption is apparent over a 6,000 gauss field range. The prominent feature is a broad asymmetrical peak at $g = 2.0$. Furthermore, this peak broadens with increased gadolinium concentration until, with the pure oxide specimen, an almost featureless trace is obtained. The reason for this broadening is not clear at present but a contributory factor is almost certainly the dipole – dipole interactions present at the concentrations used. In addition to this most obvious feature there is a peak at $g = 5.40$ with a hint of another peak at approximately $g = 2.88$.

The calculated energy levels for the Hamiltonian given on page 50 are shown graphically in Figure 7.5 for $\lambda = {}^{E}/D = 0.3$. The three diagrams are for the external $\underline{H}$ field taken to be along the x, y and z directions. The left side of each diagram corresponds to the strong Zeeman case, with eight equally spaced energy levels. The right side of each diagram corresponds to the strong crystal field case, with four pairs of energy levels. The energies are in units of $\mu_B H$ so that
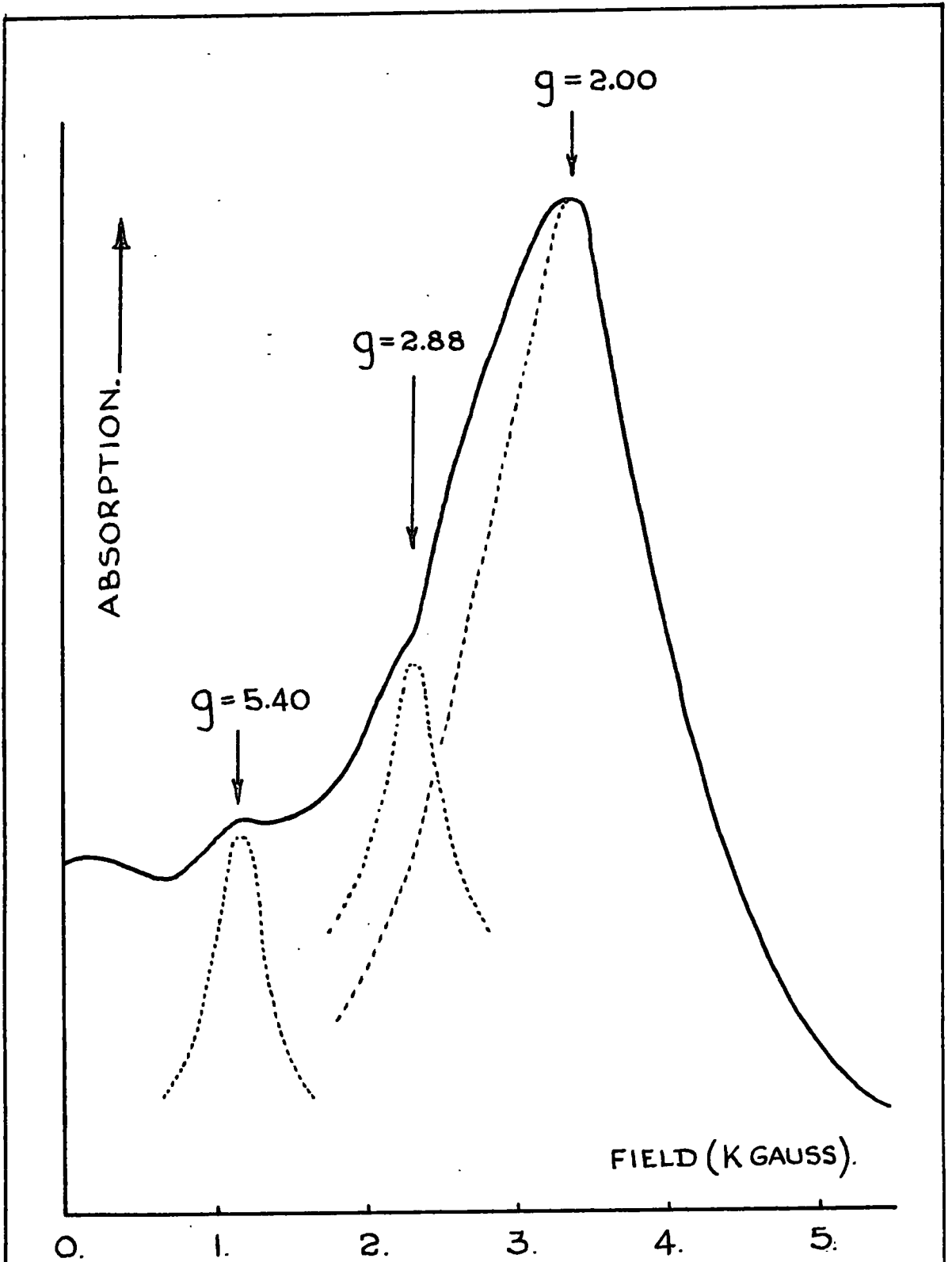
ABSORPTION CURVE FOR A SODA GLASS SPECIMEN
CONTAINING 5% (BY WT.) GADOLINIUM OXIDE.

FIG. 7.1

g = 2.00

g = 2.88

g = 5.40

ABSORPTION.

FIELD (K GAUSS).

0.   1.   2.   3.   4.   5.

ABSORPTION CURVE FOR A SODA GLASS SPECIMEN
CONTAINING 10% (BY WT.) GADOLINIUM OXIDE.

FIG. 7.2

ABSORPTION CURVE FOR A PURE GADOLINIUM OXIDE SPECIMEN.

FIG. 7.3
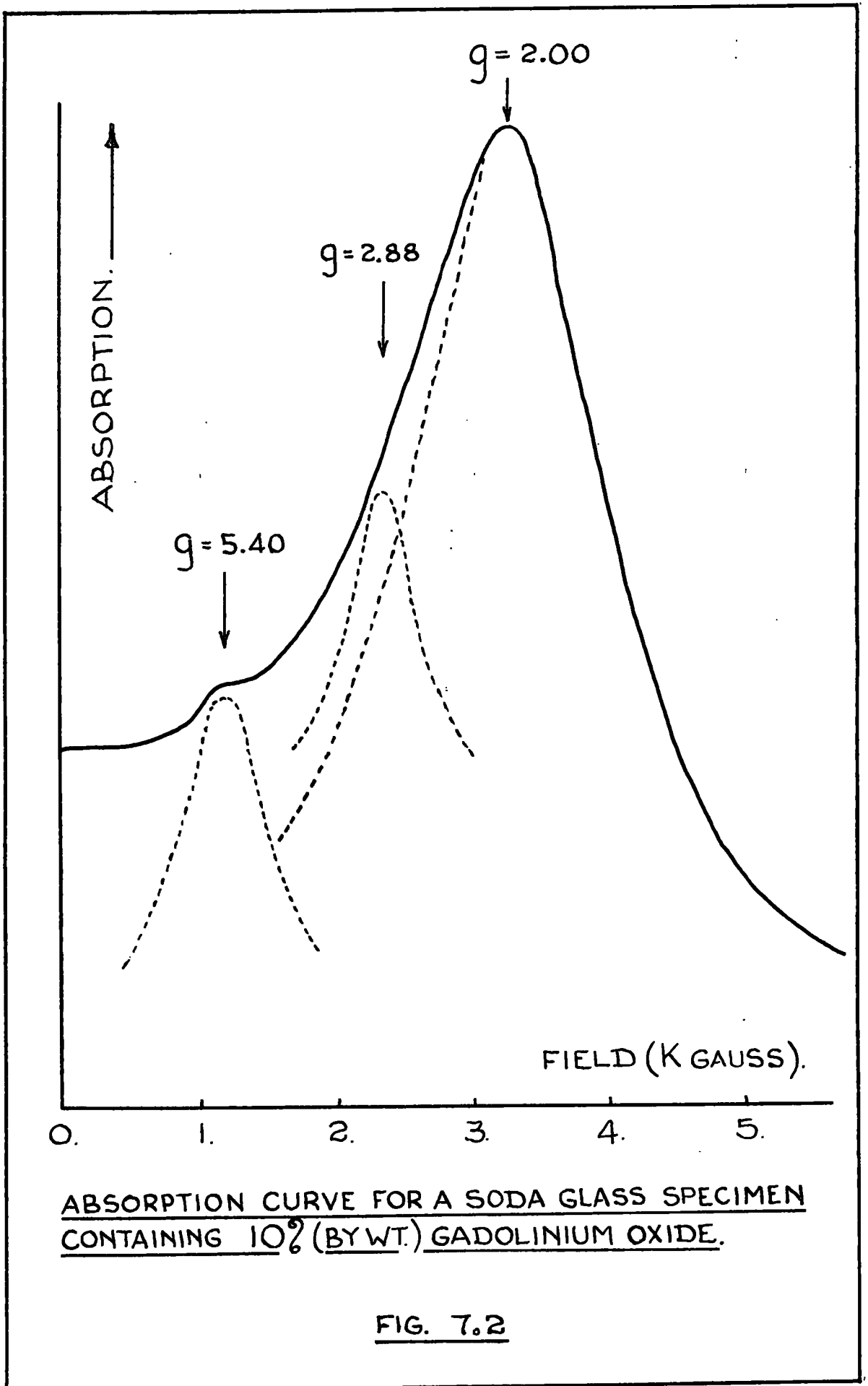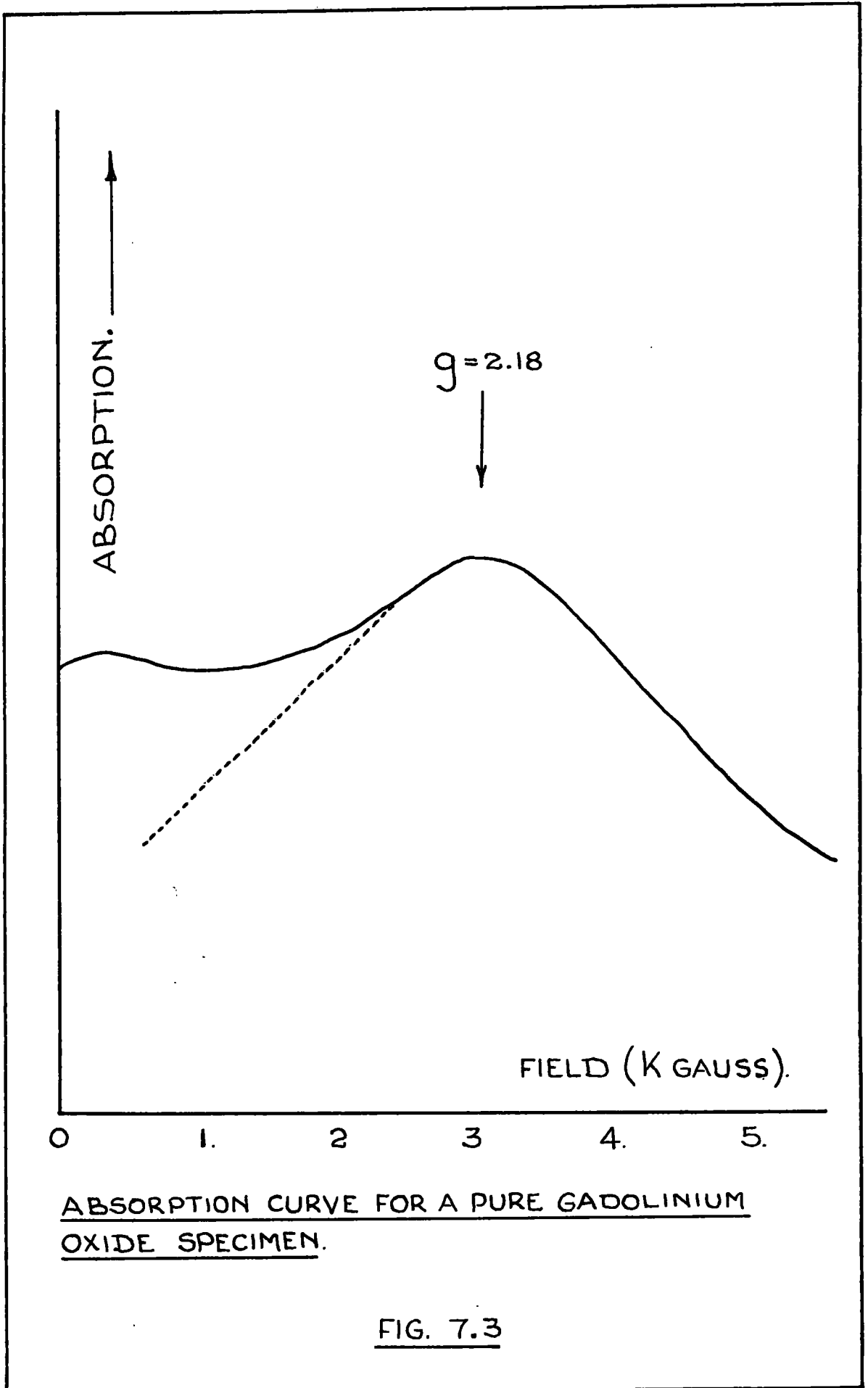
the effective g value for a transition is given directly by the difference of the two levels involved. The levels are considered to be labelled 1 to 8 from highest energy to lowest energy, starting at the left hand side of each diagram. This labelling is carried through for all values of crystal field strength. Thus, for example, level 3y drops below level 4y in the region around $D/\mu_B H = 0.75$ and then crosses level 4y again at $D/\mu_B H = 1.13$ and remains above level 4y as $D/\mu_B H$ increases.

As mentioned earlier, the energy levels given in Figure 7.5 are in units of $\mu_B H$ so that the difference between levels gives the effective g value for the transition directly. Since we have, by definition

$$h \nu = g\mu_B H$$

the results of the calculations can be summarized on a single graph derived from the energy levels. This is done by effectively normalizing the crystal field and Zeeman field by dividing $D/\mu_B H$ and g_o by the effective g. This gives

$$D/g\mu_B H = D/h\nu$$

for the abscissa and g_o/g for the ordinate. This essentially plots the magnetic field at which a transition occurs on the vertical axis increasing from 0 versus crystal field strength on the horizontal axis. This is shown in Figure 7.6.

An additional scale which gives g directly has been included.

By fitting the experimental data to this family of graphs the appropriate value of $D/h\nu$ is 0.21 for the microwave frequency used. This gives crystal field parameters

$$D = 2.06 \quad \text{and} \quad E = 0.62.$$

The g = 2 resonance is caused by 2 - 3y, 4 - 5y, and 4 - 5z transitions. The feature at g = 2.88 is caused by 5 - 6y and 3 - 4z transitions and the g = 5.4 resonance apparently comes from the 6 - 7y transition and a 2 - 3z transition could cause the low field side broadening of this peak. The transitions 2 - 3y, 3 - 4y, 5 - 6z, 1 - 2x and 7 - 8x account for the featureless tail on the high field side of g = 2 since they are distinctly non-stationary with respect to $D/\mu_B H$.

The comparison drawn in Table 7.1 shows a close relationship between the results obtained in this research and those published by Nicklin in 1967.

	ν (GHz)	Effective g values of features		
This research	9.30	2.0	2.88	5.40
Literature	9.81	2.0	2.82	5.89

Table 7.1

Erratum: In FIG. 7.5 for βH read $\mu_B H$.

CRYSTAL FIELD D/βH.
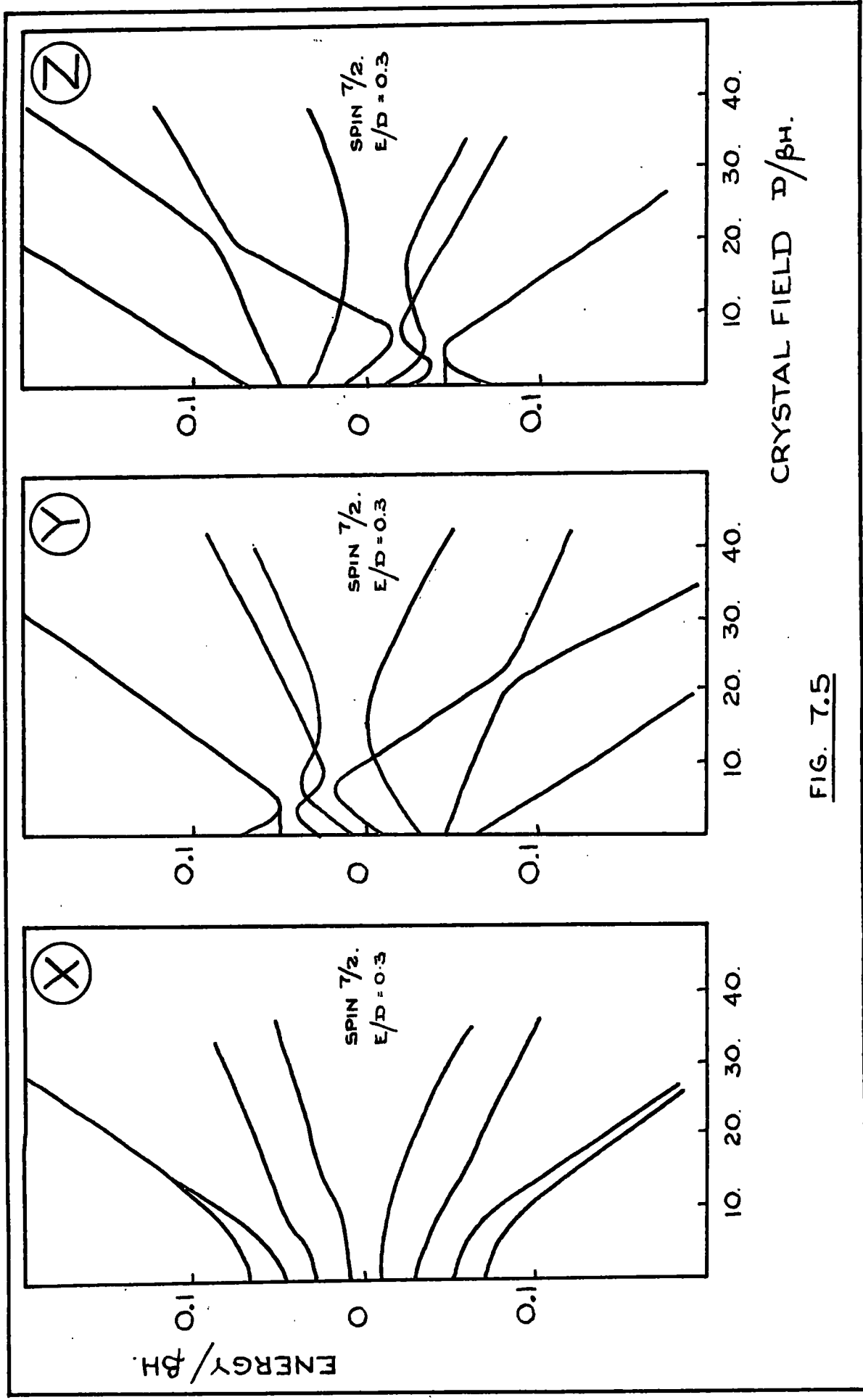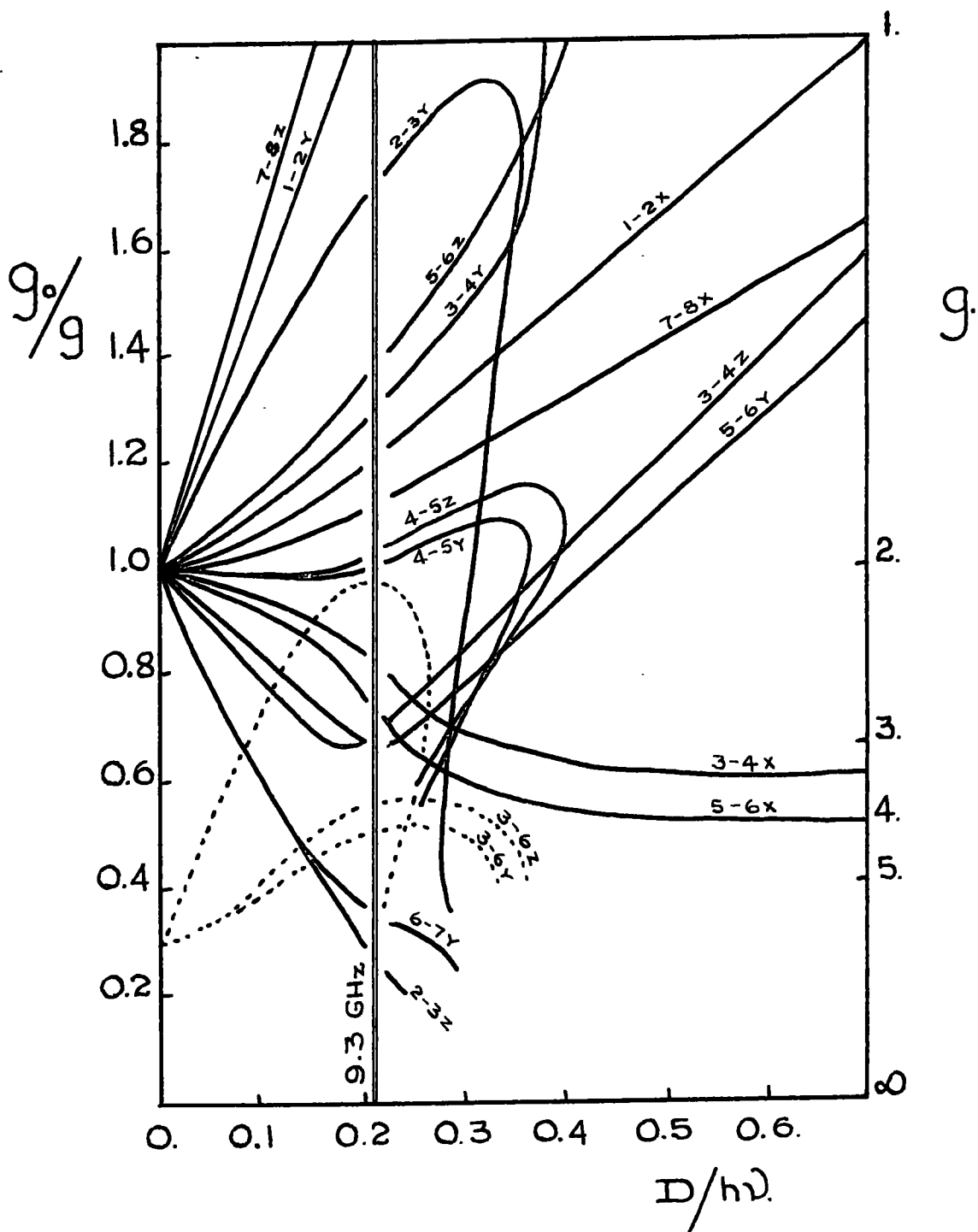
FIG. 7.5

ENERGY/βH.

X
SPIN 7/2.
E/D = 0.3

Y
SPIN 7/2.
E/D = 0.3

N
SPIN 7/2.
E/D = 0.3

THIS LINE, AT D/hν = 0.21, LOCATES
THE PRINCIPAL FEATURES OF A
TYPICAL X-BAND SPECTRUM.

FIG. 7.6

Thus, using the spin Hamiltonian previously quoted, we have accounted for the major spectral features of the Gd^{3+} ion in surroundings where the effect of the crystal field cannot be treated as a perturbation except at very high microwave frequencies.

7.6 The Siting of the Gd^{3+} ion in a Glassy Structure.

The size of the Gd^{3+} ion and its coordination number of 6 or 8 with oxygen precludes its substitution for silicon in the tetrahedra. This means that the ion must seek a position in the space left by the structural silica tetrahedra.

Electron microscopy work (30) has shown that there are regions in $LiO_2 - SiO_2$ glasses that are lithium rich. This picture of heterogeneity, applied to soda glass, would suggest regions where alkali ions concentrate in the silicon poor regions of the structure. Nicklin suggests that the Gd^{3+} ions fit themselves into the spaces created between these more complex alkali rich structures. As evidence he sites the fact that a specimen containing only silica and gadolinium oxide exhibits only a weak resonance at g = 5 and a very broad smear of absorption intensity. This indicates that the ion in these surroundings experiences very strong crystal field effects, with such a range of distortions that only an energy level situation that can give rise to an

isotropic g value could give a resolvable peak. On the other hand, the addition of even 0.5% Na_2O ($4Na^+$: $1Gd^{3+}$) changed the spectra dramatically and it is evident that, although the pattern is still very broad, the Na^+ ions must be responsible for a more definite crystal field strength at the Gd^{3+} sites. Since this behaviour persists even though the ratio Na^+/Gd^{3+} is reduced to $1/5$ one is lead to the conclusion that regions of Na^+ ion concentration must exist if the spectra are to remain unaffected by the variation. It would appear that the Gd^{3+} ion seeks out sites that provide it with a reasonably uniform crystal electric field which, in the case of the base glass used in this investigation, must lie between the alkali rich regions in the structure.

In order to understand the results described in this and the previous section, it is desirable that similar studies be made of gadolinium ions dispersed in an insulating single crystal matrix. The most closely related material which might be used for this purpose would appear to be Gd_2O_3.

CONCLUSION.

As a result of these measurements it is clear that,for

a future study of glass systems using rare earth probes,

experiments involving either optical or E.S.R. measurements

will provide most information about the glass matrix. Once

this has been done it should be possible to use the

information so derived to calculate theoretical values of

susceptibility for comparison with results of the type given

in Chapter Five.

The electrical conductivity, whilst being of great

interest, is less likely to provide direct structural

information since its value depends upon so many parameters.

However, the apparent dependence of the resistivity

behaviour on the ionic moment of the dissolved ions is

extremely interesting and requires further investigation

along the lines indicated in Chapter Four.

APPENDIX I.

CHEMICAL ANALYSIS OF THE SODA GLASS USED IN THE SPECIMEN PREPARATION.

	%
SiO_2	70.78
Al_2O_3	2.36
MgO	2.36
CaO	4.95
BaO	1.76
Na_2O	16.40
K_2O	1.60
PbO	0.10
B_2O_3	Nil

Fe	
Mn	Trace
Ti	
Cu	

This quantitative analysis was carried out by Mr. J. Sanderson at the

British Steel Corporation (Consett) laboratories using standard wet

chemical techniques.
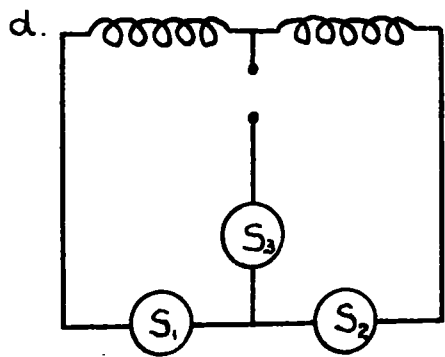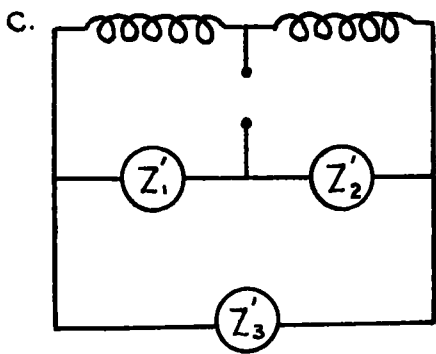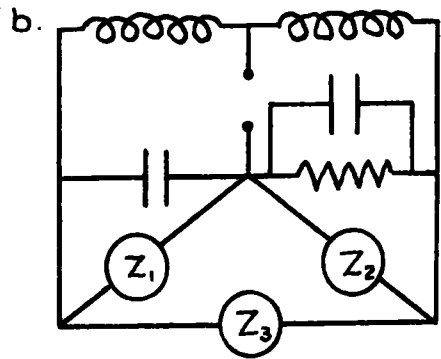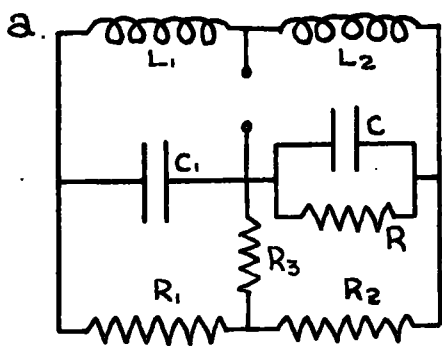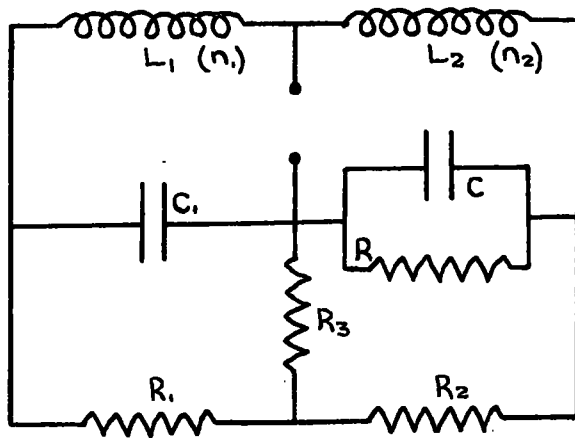
THE A.C. BRIDGE TRANSFORMATIONS.

APPENDIX II.

### THE BALANCE CONDITIONS FOR THE A.C. BRIDGE.

The circuit of the A.C. bridge used to obtain the resistivity measurements of Chapter Four is shown on the previous page.

It is not possible to derive the balance conditions easily, by the use of Kirchoff's Laws, since the algebraic equations become somewhat cumbersome. By applying the star - delta transformation method however, the balance relations may be readily obtained.

The star - delta transformation states that any three terminal impedance network of the star form
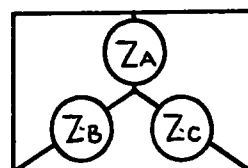
may be rewritten in the delta form
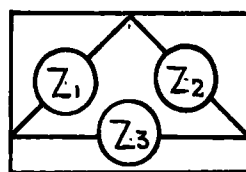
in which the impedances are given by the equations

$$Z_1 = Z_B Z_C \left(\frac{1}{Z_A} + \frac{1}{Z_B} + \frac{1}{Z_C} \right)$$

$$Z_2 = Z_A Z_C \left(\frac{1}{Z_A} + \frac{1}{Z_B} + \frac{1}{Z_C} \right) \qquad \Bigg\} \quad \text{------- A.1}$$

$$Z_3 = Z_A Z_B \left(\frac{1}{Z_A} + \frac{1}{Z_B} + \frac{1}{Z_C} \right)$$

APPENDIX II (contd.)

Conversely the reverse transformation may be obtained with the relations:

$$Z_A = Z_3 Z_1 / (Z_1 + Z_2 + Z_3)$$

$$Z_B = Z_1 Z_2 / (Z_1 + Z_2 + Z_3)$$

$$Z_C = Z_2 Z_3 / (Z_1 + Z_2 + Z_3)$$

$$\left. \right\} \quad \text{---------A.2}$$

Using these transformations, the balance conditions are easily found. In the Figure showing the A.C. bridge transformation, the step a to b is carried out using the equations A.1 and gives that

$$Z_1 = R_1 R_3 \left(\frac{1}{R_3} + \frac{1}{R_2} + \frac{1}{R_1} \right)$$

$$Z_2 = R_2 R_3 \left(\frac{1}{R_3} + \frac{1}{R_2} + \frac{1}{R_1} \right)$$

$$Z_3 = R_1 R_2 \left(\frac{1}{R_3} + \frac{1}{R_2} + \frac{1}{R_1} \right)$$

The circuit may then be redrawn as in c, where

$$Z_1^1 = Z_1 / (1 + j\omega C_1 Z_1)$$

$$Z_2^1 = Z_2 R / (R + Z_2 + j\omega C R Z_2)$$

$$Z_3^1 = Z_3$$

Using the A.2 equations for the step c to d we then have:

$$S_1 = Z_1^1 Z_3^1 (Z_1^1 + Z_2^1 + Z_3^1)$$

$$S_2 = Z_2^1 Z_3^1 (Z_1^1 + Z_2^1 + Z_3^1)$$

$$S_3 = Z_1^1 Z_2^1 (Z_1^1 + Z_2^1 + Z_3^1)$$

APPENDIX II (contd.)

Now figure d of the A.C. bridge transformations is a simple Wheatstone network for which the balance condition is

$$\frac{S_1}{S_2} = \frac{S_4}{S_5} = \frac{j\omega L_1}{j\omega L_2} = \frac{n_1}{n_2}.$$

and from the previous relations

$$\frac{n_1}{n_2} = \frac{S_1}{S_2} = \frac{Z_1^{\,1}}{Z_2^{\,1}} = \frac{Z_1(R + Z_2 + j\omega CRZ_2)}{(1 + j\omega C_1 Z_1)\, Z_2 R}$$

Expanding this expression and simplifying, then gives that

$$n_1\left[RR_2 + j\omega C_1(R_1 R_2 + R_2 R_3 + R_1 R_3)\right] = n_2\left[RR_1 + R_1 R_2 + R_2 R_3 + R_1 R_3 + j\omega CR(R_1 R_2 + R_2 R_3 + R_1 R_3)\right]$$

and by equating the real and imaginary parts, the balance conditions become

$$\frac{n_1}{n_2} = \frac{R_1 R_2 + R_2 R_3 + R_1 R_3 + RR_1}{RR_2} = \frac{C}{C_1}$$

REFERENCES.

1. Zachariasen W.H.   J.Amer.Chem.Soc. 54 3941 (1932)

2. Bragg W.L.   Ceram.Abs. 17 231 (1938)

3. Randall J.T.   Z.Krist. 75 196 (1930)

4. Valenkov N. & Porai-Koshits. Z.Krist. 95 195 (1936)

5. Warren B.E. & Biscoe J.   J.Amer.Ceram.Soc. 21 49 (1938)

6. Evans P.L. & King S.V.   Nature 212 1353 (1966)

7. Glass Engineering Handbook (2nd Ed.) McGraw-Hill

            Book Co. Inc.   (1958)

8. Biscoe J.   J.Ceram.Soc. 24 262 (1941)

9. Kraus C.A. & Darby E.H.   J.Amer.Chem.Soc. 44 2783 (1922)

10. Peyches I.   Silicates Ind. 21 209 (1956)

11. Fulda M.   Sprechsaal 60 769 (1927)

12. Rasch E. & Hindrichsen F.W.   Z.Electrochem. 14 41 (1908)

13. Blumlein A.D.   British Patent No. 323037

14. Clark H.A.M. & Vanderlyn P.D.   Proc. I.E.E. 96 (Pt.II)

                        365 (1949)

15. Elliott R.J. & Stevens K.W.H.   Proc.Roy.Soc. A218 533

                                    (1953)

16. Ruderman M.A. & Kittel C.   Phys.Rev. 96 99 (1954)

    Yosida K.   Phys.Rev. 106 893 (1957)

    Kasuya T.   Prog.Theoret.Phys.(Kyoto) 16 45 (1956)

65.

17.   Zijlstra H.   "Experimental Methods of Magnetism" Part II

                North Holland Publishing Co. (1967)

18.   Selwood P.W.   "Magnetochemistry" Interscience

                Publishers Inc. (1943)

19.   Schieber M.M.   "Experimental Magnetochemistry"

                North Holland Publishing Co. (1967)

20.   Henderson J.R., Muramoto M. & Gruber J.B.

                J. Chem. Phys. $\underline{46}$ 2515 (1967)

21.   Lell E., Kreidl N.J. & Hensler J.R.

                Progr. in Ceram. Sc. $\underline{4}$ 1 (1966)

22.   Sands R.H.   Phys. Rev. $\underline{99}$ 1222 (1955)

23.   Castner T., Newell G.S., Holton W.C. & Slichter C.P.

                J. Chem. Phys. $\underline{32}$ 668 (1960)

24.   Chapeleva I.V., La zukin V.N. & Dembovskii S.A.

                Soviet Physics - Doklady $\underline{11}$ 864 (1967)

25.   Griscom D.L., Bray P.J. & Griscom R.E.   U.S. Atomic

                Energy Commission Report NYO-2024-11 (1967)

26.   Nicklin R.C.   Ph.D. Thesis, Iowa State Univ. (1967)

27.   Pake G.E.   "Paramagnetic Resonance"   W.A. Benjamin Inc.

                                            (1962)

28.   Stanworth J.F.   "Physical Properties of Glass"

                Clarendon, Oxford. (1950)

29.   Rebbeck J.W., Mulligan M.J. & Ferguson J.B.

                J. Amer,Ceram.Soc. $\underline{8}$ 329   (1925)

30.   Vogel W.   Structure of Glass $\underline{6}$ 114   (1966)